Wnt- and Glutamate-receptors orchestrate stem cell dynamics and asymmetric cell division

Sergi Junyent*[,1], Joshua Reeves*[,1], James L. A. Szczerkowski[1], Clare L. Garcin[1], Tung-Jui Trieu[1], Matthew Wilson[1], Jethro Lundie-Brown[1] and Shukry J. Habib[#,1]

*These authors contributed equally

[#]Correspondence to: shukry.habib@kcl.ac.uk

[1]Centre for Stem Cells and Regenerative Medicine, King's College London. 28th Floor, Tower Wing, Guy's Campus, Great Maze Pond, SE1 9RT. London, United Kingdom.

ABSTRACT

The Wnt-pathway is part of a signalling network that regulates many aspects of cell biology. Recently we discovered crosstalk between AMPA/Kainate-type ionotropic glutamate receptors (iGluRs) and the Wnt-pathway during the initial Wnt3a-interaction at the cytonemes of embryonic stem cells (ESCs). Here, we demonstrate that this crosstalk persists throughout the Wnt3a-response in ESCs. Both AMPA- and Kainate-receptors regulate early Wnt3a-recruitment, dynamics on the cell membrane, and orientation of the spindle towards a Wnt3a-source at mitosis. AMPA-receptors specifically are required for segregating cell fate components during Wnt3a-mediated asymmetric cell division (ACD). Using Wnt-pathway component knockout lines, we determine that Wnt co-receptor Lrp6 has particular functionality over Lrp5 in cytoneme formation, and in facilitating ACD. Both Lrp5 and 6, alongside pathway effector β-catenin act in concert to mediate the positioning of the dynamic interaction with, and spindle orientation to, a localized Wnt3a-source. Wnt-iGluR crosstalk may prove pervasive throughout embryonic and adult stem cell signalling.

INTRODUCTION

Cell to cell communication is fundamental to multicellular life. Developmental signals critical for tissue patterning and formation are traditionally considered as diffuse signals that pervade the extracellular matrix. However, signals have often been found to be delivered to target cells or received from source cells via specialized signalling filopodia — cytonemes (Kornberg and Roy, 2014).

Stem cells, both embryonic and adult, regulate tissue formation. Many stem cells rely on Wnts as signals for self-renewal and differentiation in the balance of cell fate determination during development, tissue homeostasis and disease (Garcin and Habib, 2017). Wnt ligands bind receptor Fzd, alongside co-receptors Lrp5 or Lrp6, ultimately leading to β-catenin–dependent transcription of target genes. In several systems (Bertrand, 2016; Goldstein et al., 2006; Huang and Niehrs, 2014; Kaur et al., 2020; Sugioka et al., 2011; Walston et al., 2004), including mouse embryonic stem cells (ESCs) (Habib et al., 2013), localized Wnts induce oriented asymmetric cell division (ACD).

As cultured single cells that retain the capacity to self-renew and differentiate to all adult lineages, ESCs are an ideal experimental system for studying cell fate determination (Martello and Smith, 2014). By combining ESCs and trophoblast stem cells (TSCs) to generate 3D structures that resemble the developing embryo, we recently identified ESC-generated cytonemes that mediate the interaction with Wnt-secreting TSCs (Junyent et al., 2021, 2020). To overcome the multiplicity of signals and the difficulty in visualising secreted Wnt ligands, we used Wnt3a tethered to microbeads, showing that ESC-cytonemes selectively recruit self-renewal-promoting Wnt3a ligands. Cytonemes interacting with localised Wnt3a signals engage not only Wnt-receptors, but also ionotropic AMPA/Kainate-type glutamate receptors (iGluRs) (Junyent et al., 2021, 2020). Consequently, rapid calcium (Ca^{2+}) transients are generated at the cytoneme, leading to Wnt3a reactivity: Wnt3a-bead recruitment to the cell body (soma), activating Wnt/β-catenin signalling and promoting asymmetric cell division (ACD) of markers of cell fate (Habib et al., 2013).

iGluRs are primarily studied in excitatory glutamatergic synapses between neurons, however they are increasingly being found in other cell types, such as stem cells (Genever et al., 1999; Morhenn et al., 1994; Skerry and Genever, 2001) and functioning in *Drosophila* development (Huang et al., 2019). AMPA- and Kainate-type iGluRs are tetrameric glutamate-sensitive (amongst other ligands (Traynelis et al., 2010)) ion channels. AMPA/Kainate-receptors require subunits GriA3 and GriA4, or GriK1 and GriK3 to function, respectively (Cull-Candy et al., 2006; Lerma and Marques, 2013). Activation increases their ion permeability, inducing rapid ion influxes critical to signal transmission.

However, it remained unknown how the interconnected roles of Wnt-pathway and AMPA/Kainate-receptor components influence highly dynamic Wnt3a interactions, and the subsequent Wnt3a-mediated ACD of ESCs.

Here, we resolve the dynamics of localized Wnt3a ligand (Wnt3a-bead) recruitment by single ESCs into three stages: initial cytoneme-mediated interactions; Wnt3a-bead interaction with the cell membrane; and the subsequent effects of the Wnt3a-bead recruitment on spindle orientation and cell fate determination. We generated ESCs knocked-out (KO) for the AMPA- and Kainate-type iGluRs by double knock-out (dKO) of critical protein subunits (AMPA: GriA3/4dKO; Kainate: GriK1/3dKO). Multiple clonal cell lines were investigated alongside pharmacological inhibition, both previously- and newly-generated mutants for Wnt co-receptors (Lrp5, Lrp6 and Lrp5/6 dKO (Junyent et al., 2020)), and inducible β-catenin KO ESCs (Raggioli et al., 2014)).

We show that while Lrp6, β-catenin and AMPA/Kainate-receptors are required for the population-wide cytoneme-mediated uptake of Wnt3a-beads, neither AMPA- nor Kainate-receptors are important to the formation of cytonemes themselves. Lrp5, conversely, has an inhibitory role in regulating cytoneme generation in single ESCs and Wnt3a-bead accumulation at cell-population level. In WT ESCs, Wnt3a ligands are recruited from initial cytoneme interaction site at the cell periphery, towards the centre of the cell soma, a process which requires Lrp5, Lrp6, β-catenin, AMPA- and Kainate-receptors. Upon progression to mitosis, WT ESCs orient the spindle towards Wnt3a-beads but not inert (chemically inactivated) iWnt3a-beads. Cells lacking Lrp5, Lrp6, β-catenin, AMPA- or Kainate-receptors have significantly impaired ability to orient the spindle towards the Wnt3a signal source.

WT ESCs divide asymmetrically in response to a Wnt3a-bead, producing a self-renewed proximal ESC cell and a distal cell that is prone to differentiation (Habib et al., 2013). Specifically, we demonstrate that Lrp5 is not required in Wnt3a-mediated ACD, while Lrp6 and β-catenin are crucial. Importantly, we distinguish that AMPA-receptors, but not Kainate-receptors, are critical in the cell fate determination of Wnt3a-mediated ACD in ESCs.

Taken together, we show that AMPA/Kainate-type iGluR activity is incorporated throughout the interaction of ESCs with localized Wnt3a signals. We dissect the dynamic interaction of Wnt3a-ligand with ESC, from initial uptake to cellular division, showing that its efficient regulation requires Wnt co-receptors and downstream β-catenin in concert with AMPA/Kainate-receptor activity. Our multiple clone approach to component KOs suggests that the downstream cellular responses to localized Wnt3a of spindle orientation and asymmetric cell division are impervious to clonal variation in the initial dynamics of the

Wnt3a-interaction. Through this, we specify novel differences between the roles of Lrp5 and 6, and between AMPA- and Kainate-type iGluRs in the response to localized Wnt3a.

RESULTS

Wnt co-receptors and β-catenin regulate Wnt3a-bead accumulation by modifying the cytonemes of ESCs

We aimed to investigate how components of the Wnt/β-catenin pathway (**Fig. 1A**) affect the cellular dynamics of ESCs and their capacity to respond to localized Wnt3a ligands. We used our previously generated ESC lines knocked-out (KO) for the co-receptors of the Wnt/β-catenin pathway: Lrp5 (Lrp5KO), Lrp6 (Lrp6KO) or both Lrp5 and 6 double KO (Lrp5/6dKO) (described in (Junyent et al., 2020), here named KO #1). An additional clone of each line was newly generated to investigate the influence of clonal variation during the interaction with Wnt3a signals (named KO #2, **Fig. 1 – Figure Supplement 1**). We also used an ESC line with a conditional KO of the pathway effector, β-catenin (βKO) (generated as described in (Junyent et al., 2020; Raggioli et al., 2014)).

To validate the response of the clones of the KO cell lines to exogenous Wnt3a ligands, we used cells harbouring the Wnt/β-catenin pathway reporter, 7xTCF-eGFP, in which eGFP is expressed upon pathway activation (Fuerer and Nusse, 2010) (**Fig. 1B and C**). Similar to our previous findings (Junyent et al., 2020), in the presence of solubilized Wnt3a ligands 49.07% of wild-type (WT) cells express eGFP, while only a basal level of pathway activation is observed in these cells in the absence of Wnt3a (**Fig. 1C**). In comparison, Lrp5KO ESCs have a significant reduction in pathway activation in response to Wnt3a (26.97% $eGFP^+$ cells). In Lrp6KO ESCs, pathway activation is further compromised (5.61% $eGFP^+$ cells). Lrp5/6dKO and βKO ESCs cannot activate the Wnt/β-catenin pathway in response to solubilized Wnt3a addition (**Fig. 1B and C**). We also measured the expression of *Axin2* (a universal Wnt/β-catenin target gene) in WT or KO ESCs stimulated with soluble Wnt3a. Again, this demonstrated a reduction in Wnt/β-catenin pathway activation in Lrp5KO and Lrp6KO ESCs, and the absence of responsiveness to Wnt3a in Lrp5/6dKO or βKO cells (**Fig. 1D**).

At the single cell level, ESCs use dynamic cytonemes to contact and recruit Wnt3a ligands immobilized to a microbead (Wnt3a-beads) (Junyent et al., 2021, 2020). These cytonemes are shorter in βKO and Lrp6-mutant ESCs (Lrp6KO, Lrp5/6dKO) than in WT ESCs, and are presented in greater numbers in βKO cells (Junyent et al., 2020) (exemplified in **Fig. 1E, Figure 1 – Figure Supplement 2**, **Movies 1-5**).

To investigate how differences in Wnt3a-response and single-cell behaviours affect the accumulation of Wnt3a-beads at the population level over a prolonged period, we cultured ESCs at low density and presented them with dispersed Wnt3a-beads. In some conditions, we presented the cells with inactivated Wnt3a-beads (iWnt3a-beads), dithiothreitol (DTT)-treated to denature the Wnt3a protein while covalently bound to the bead. Cells were then live-imaged each minute for a total of 12 hours and the percentage of cells with cytonemes as well as the proportion of cells contacting Wnt3a-beads were analysed.

WT ESCs begin forming cytonemes upon substrate attachment: within 4 hours, over 40% of WT ESCs had cytonemes (**Fig. 2A**). This was coupled with a linear increase in the proportion of WT ESCs with beads in the first 4 hours of imaging, rising to 54.1% by 4h, and 63.5% by 11 hours (**Fig. 3A**). ESC cytonemes are ligand-selective and can efficiently recruit localized Wnt3a signals but not iWnt3a-beads (Junyent et al., 2020). Indeed, the percentage of WT ESCs with iWnt3a-beads did not rise and remained less than 20% for most of the time period (**Fig. 3A**).

Interestingly, >56% of Lrp5KO ESCs generate cytonemes in 3 hours, more than WT ESCs (**Fig. 2A**). These cells retained the ability to quickly accumulate Wnt3a-beads, reaching ~50% cells with beads after 3h and an overall mean of 61.5% after 6 hours (**Fig. 3B**). The rate of increase in the percentage of Lrp6KO (**Fig. 2B**), Lrp5/6dKO (**Fig. 2C**) and βKO ESCs (**Fig. 2D**) with cytonemes is largely similar to WT, with some clonal variability in the Lrp6KO cells (**Fig. 2B**). Cytonemes of single ESCs lacking Lrp6 (Lrp6KO, Lrp5/6dKO) exhibit reduced reactivity – decreased Wnt3a-bead uptake following initial contact (Junyent et al., 2020). Indeed, Lrp6KO and Lrp5/6dKO showed long-term impaired Wnt3a-bead accumulation at the population level, remaining at ~33% cells with beads over the course of 12 hours. This resembled the interaction of WT cells with iWnt3a-beads (**Fig. 3C, D and F**). While cells lacking β-catenin (βKO) retain the capacity to efficiently recruit Wnt3a signals in single-cell–single-bead interactions (Junyent et al., 2020), they had significantly impaired long-term Wnt3a-bead accumulation at the population level, reaching a maximum mean of 32.7% cells with beads after 12 h (**Fig. 3E and F**).

Together with cytoneme formation, cell motility provides a mechanism to encounter and interact with the local environment. To understand whether cytoneme formation or Wnt3a-bead accumulation is coupled to cellular motility, we calculated the Mean Squared Displacement per minute (MSD), the average movement per minute, of single cells. Cell motility in WT ESCs is minimal, with a median MSD of 1.08 μm^2/min (**Fig. 2E**). No significant differences to WT were observed between receptor or β-catenin KO ESCs, with the median MSD for each cell type falling between 0.74 and 1.36 μm^2/min (**Fig. 2E**).

Altogether, we observed that intrinsic Wnt/β-catenin components control the generation and function of cytonemes without affecting overall cellular motility. Single cell effects, such as shortening of the cytonemes (in βKO ESCs) or changes in the functionality of the cytonemes (Lrp6KO, Lrp5/6dKO ESCs, or WT ESCs contacting iWnt3a beads) are reflected in population-level changes in the rate of Wnt3a signal accumulation over a prolonged period.

Despite these differences, it is important to note that, in all conditions, some cells do take up and retain Wnt3a-beads, allowing further analysis of the interaction with localized Wnt3a.

Wnt3a-bead positioning at the membrane is controlled by Wnt co-receptors and β-catenin

Cytoneme-mediated Wnt3a recruitment is the first stage in the process of signal reception, followed by a period of dynamic cell-signal interaction at the membrane of ESCs. Unless interrupted by the loss of contact (Wnt3a-bead dropping) (**Fig. 4A**), this interaction often persists until cell division. The positioning of the signal-receptor complexes on the plasma membrane has been shown to affect signalling activity (Rangamani et al., 2013)(Schmick and Bastiaens, 2014). The Wnt3a-bead approach provides a unique opportunity to quantify the dynamics and positioning of localized Wnt3a on the cell membrane, as well as the roles of the Wnt pathway co-receptors and β-catenin in its regulation. Therefore, we next analysed the interaction of Wnt3a-bead and ESCs after initial cytoneme-mediated recruitment.

We followed cells that recruit a Wnt3a-bead with a cytoneme for 3h (180 min) after Wnt3a-bead recruitment, a time point sufficient to measure the kinetics of initial cell-signal interaction, and activate the downstream β-catenin related machinery of the pathway (Hernandez et al., 2012)(**Movie 6**). We measured the distance between the Wnt3a-bead and the cell centre, reporting it as a proportion of the cell radius (**Fig. 4B**).

WT ESCs initially recruit Wnt3a-beads with a cytoneme, and rapidly relocate them from the tip to the membrane at the base (between 0.7 and 1.0 of the cell radius), then closer to the cell centre (between 0.3 and 0.7 of the cell radius). Within 1 hour, Wnt3a-beads were, on average, at ~0.5 of the cell radius (**Fig. 4B and C, Figure 4 – Figure Supplement 1, Movie 6**). iWnt3a-beads are also initially moved from the WT ESC cytoneme tip to the periphery (0.7 to 1.0 of the cell radius). However, iWnt3a-beads are not positioned further towards the cell centre, reaching at closest ~0.7 of the cell radius, on average (**Fig. 4B and C**).

ESCs lacking Lrp6 (Lrp6KO, Lrp5/6dKO) or β-catenin are likewise, on average, largely unable to position the Wnt3a-bead closer to the cell body (**Fig. 4B and E-G, Movie 6**). In these conditions the bead is stabilized after 90 min in mean positions ranging from 0.62 to 0.70 for Lrp6KO and Lrp5/6dKO, to ~0.70 for βKO ESCs. Lrp5KO ESCs position the Wnt3a-

beads at approximately 0.6 after 120 minutes, further from the centre of the cell than WT ESCs (**Fig. 4D**), with clonal differences in the initial positioning.

The dynamics of Wnt3a-cell interaction are also defined by the speed of Wnt3a-bead movement relative to the cell. Thus, we also calculated the MSD of the bead relative to the centre of the cell (**Fig. 4H**). iWnt3a-beads held by WT ESCs have a higher rate of movement than Wnt3a-beads, with a median MSD of 4.02 μm^2/min versus 3.08 μm^2/min for Wnt3a-beads (**Fig. 4I**). In mutant ESCs contacting Wnt3a-beads, differences in Wnt3a-bead movement are largely clone-dependent and independent of the genotype of the cell, with the median MSD ranging between 4.25 μm^2/min in Lrp5KO (#1) and 2.61 μm^2/min in Lrp5/6dKO (#2) (**Fig. 4I**).

Finally, we investigated whether positioning of the Wnt3a-bead further from the cell centre lead to shorter Wnt3a-cell interactions. We observed that, within the first 3 hours of interaction following cytoneme-recruitment, WT ESCs drop iWnt3a-beads at a significantly higher rate than Wnt3a-beads (44.4% versus 4.08%, **Fig. 4J**). However, most mutant ESCs that succeed in recruiting Wnt3a-beads retain them, with rates ranging between 100% of cells retaining beads in Lrp5KO #2 and 80.4% cells retaining beads in Lrp6KO #2 (**Fig. 4J**).

Altogether, our results show that WT ESCs recruit and retain Wnt3a-beads at the membrane, where they are positioned near the centre of the cell with limited movement. However, WT ESCs do not recruit iWnt3a-beads efficiently and form unstable interactions with them, positioning them at the periphery of the cells, where they are also dropped at higher rates. While perturbation of the pathway components has a limited effect in recruited Wnt3a-bead movement and Wnt3a-bead retention, KO ESCs exhibit a significantly impaired ability to position Wnt3a-beads close to the centre of the cell.

AMPA/Kainate-type receptors are required for dynamic interactions with localized Wnt3a in ESCs

A crosstalk between Lrp6 and the activity of ionotropic AMPA/Kainate-type glutamate receptors (iGluRs) regulates the reactivity of ESC cytonemes to Wnt3a-beads (Junyent et al., 2021, 2020). Here, we aimed to assess whether iGluR activity might also regulate the dynamics of Wnt3a-stem cell interaction.

ESCs express the AMPA subunits GriA3 and 4, and the Kainate subunits GriK1, 2, 3 and 5 (Junyent et al., 2021, 2020). Previous publications have shown that GriA3/4 combinations can form active AMPA-receptors that channel Ca^{2+} (Brorson et al., 2004; Cull-Candy et al., 2006; Liu and Zukin, 2007), while Kainate receptor formation requires the presence of either GriK1 or GriK3 (Lerma and Marques, 2013).

To investigate the role of AMPA and Kainate iGluRs in Wnt3a-ESC interaction, we pharmacologically inhibited AMPA/Kainate iGluR activity by adding cyanquixaline (CNQX) to the media, which reduces the generation of localized, Wnt3a-mediated Ca^{2+} transients in the ESC cytonemes and impairs Wnt3a-bead recruitment (Junyent et al., 2020). To dissect the specific role of each type of receptor family, we generated ESC lines with a double KO for GriA3/4 (GriA3/4dKO, clone #1 and #2) and GriK1/3 (GriK1/3dKO, clone #1 and #2, **Fig. 5 – Figure Supplement 1**).

We initially explored the capacity of these cells to activate the Wnt/β-catenin pathway in response to exogenous Wnt3a (200 ng/mL solubilized Wnt3a or a high density of Wnt3a-beads, 6.25 μg/cm^2, **Fig. 5A-C**) after 24h. In these conditions, cells were cultured as a monolayer, and therefore Wnt3a-cell contact is cytoneme independent (**Fig. 5C**) (Junyent et al., 2021, 2020). We analysed the relative expression of *Axin2* by qPCR (for GriA3/4dKO and GriK1/3dKO) or the production of eGFP in response to 7xTCF-eGFP activation by FACS (for CNQX-treated cells). In all conditions, Wnt3a addition led to activation of the Wnt/β-catenin pathway, to levels comparable to WT (**Fig. 5A and B**).

Next, we examined whether perturbation of AMPA/Kainate-receptors by KO or pharmacological inhibition affected the capacity of ESCs to contact and recruit Wnt3a-beads. At the single cell level, both GriK1/3dKO and GriA3/4dKO ESCs generate thin dynamic cytonemes of similar number and length to WT ESCs (**Fig. 6A and B, Fig. 1 – Figure Supplement 1**, **Movie 7 and 8**). These results corroborate previous observations in CNQX-treated WT ESCs (Junyent et al., 2020), suggesting that AMPA/Kainate iGluRs do not play a role in cytoneme formation.

At the population level, GriK1/3dKO ESCs, or WT ESCs + CNQX, generate cytonemes at a rate similar to WT ESCs (approx. 44% of cells with cytonemes after 4h, **Fig. 6C, E and F**), while the percentage of cells with cytonemes in GriA3/4dKO ESCs is equal or higher than control cells (~67% after 4h for clone #2, **Fig. 6D and F**). However, Wnt3a-bead accumulation is affected in Kainate-receptor–deficient cells: GriK1/3dKO ESCs show lower Wnt3a-bead accumulation than WT ESCs, with a maximum mean of 49.5% cells with beads over the 12 hours (**Fig. 6G**). This phenotype is even more pronounced in WT ESC treated with CNQX, reaching only a mean of 39.9% of cells with Wnt3a-beads after 12h (**Fig. 6I and J**).

GriA3/4dKO ESCs show clonal variability, with clone #1 exhibiting reduced Wnt3a-bead uptake, and cells from clone #2 recruiting Wnt3a-beads at a rate similar to WT cells (**Fig. 6H and J**) This is accompanied by a significant increase in motility, with a median cell MSD of ~1.4 μm^2/min for GriA3/4dKO, compared to ~1.1 μm^2/min for WT ESCs (**Fig. 6K**).

Next, we explored the dynamics of Wnt3a-bead movement after initial recruitment by AMPA/Kainate receptor-deficient cells. Using high temporal resolution live imaging (as described in **Fig. 4B**), we observed that both GriK1/3dKO and GriA3/4dKO ESCs rapidly relocate the Wnt3a-bead from the tip of the cytoneme to the cell soma, but stabilize the position of the bead, on average, significantly further from the cell centre than WT ESCs (~0.62 of cell radius between 30 and 120 min, **Fig. 7A and B,** expanded in **Fig. 7 – Figure Supplement 1**). These cells show a slight increase in Wnt3a-bead movement, in a clone-dependent, genotype-independent manner (**Fig. 7D**). In CNQX-treated ESCs, where both AMPA and Kainate iGluRs are inhibited, the Wnt3a-beads are positioned far from the cell centre (**Fig. 7C**), and with restricted movement (**Fig. 7D**).

Collectively, our data indicates that KO or inhibition of AMPA/Kainate-type receptors, much like KO of Wnt co-receptor Lrp6 or pathway effector β-catenin, impairs Wnt3a-bead uptake and alters the dynamics of Wnt3a-ESC interaction at the cell membrane. In all conditions, importantly, once Wnt3a-cell contact has been achieved, it is often sustained until division, enabling downstream analysis of the interaction (**Fig. 7E**).

A localized Wnt3a signal can induce spindle orientation and asymmetric cell division (ACD) of single ESCs (Habib et al., 2013). We next investigated WT, Wnt/β-catenin pathway and AMPA/Kainate iGluRs KO ESCs throughout the process of Wnt3a-mediated ACD.

Wnt/β-catenin pathway components regulate the orientation of the mitotic spindle

Wnt3a-bead orients the spindle of dividing ESCs (Habib et al., 2013). Spindle orientation is an important factor in the process of ACD, in several biological systems (Bertrand, 2016; Goldstein et al., 2006; Huang and Niehrs, 2014; Kaur et al., 2020; Sugioka et al., 2011; Walston et al., 2004). Spindle orientation is established and can be determined as early as the anaphase (Kiyomitsu and Cheeseman, 2013). Therefore, we measured the angle (α) between the minor axis of mitosis and the point of bead contact, relative to the centre of division, at anaphase (**Fig. 8A and B**). In this way, 90° represents a completely Wnt3a-bead orientated division (**Fig. 8B**).

WT ESCs divide predominantly oriented towards the Wnt3a-bead, with a most common angle of 85-90° (**Fig. 8C**). This Wnt3a-biased distribution is significantly different to a randomized (Wnt3a-independent) distribution (Chi-squared test, $P<0.001$), in which division angle counts are assumed to be equally distributed between 0°-30°, 30°-60° and 60°-90°. Indeed, when presented with iWnt3a-beads, a randomized distribution of angles is observed (Chi-squared test, $P>0.05$), with an increased proportion of cells dividing with iWnt3a-beads between 0° and 5° (**Fig. 8D and L**), where the contact area is maximized and the free energy is minimized (Koltover et al., 1999).

Single ESCs that lack Lrp5, Lrp6, or β-catenin exhibit spindle misorientation (**Fig. 8E-K**), with significantly different angle distributions than WT ESCs + Wnt3a beads, as determined by two-sample Kolmogorov-Smirnov (K-S) statistical analysis (**Fig. 8L**). In these cells, most cells divide at angles ranging from 0° to 60° for Lrp5KO, Lrp6KO and Lrp5/6dKO ESCs (**Fig. 8E-J**), or with randomised angle distributions (Chi squared, P>0.05) for βKO ESCs (**Fig. 8K**).

In conclusion, disruption of the Wnt co-receptors or the downstream component β-catenin impairs the spindle orientation towards a source of localized Wnt3a during division. While localized Wnt3a controls spindle orientation, it also controls cell fate, producing a self-renewing Wnt3a-proximal ESC and a Wnt3a-distal cell prone to differentiation (Habib et al., 2013). Next, we studied whether the individual KOs affect cell fate determination during ACD.

Lrp6, but not Lrp5, is critical for asymmetric cell fate determination

ACD is the partitioning or enrichment of cellular components in one of the two daughter cells deriving from mitosis, leading to differences in their cell fate. Wnt3a-beads induce ACD in single ESCs (Habib et al., 2013). Using this system, quantifying the expression of pluripotency markers Nanog, Rex1 and Sox2 (**Fig. 9A-D**) allows the comparison of the cell fate of the daughter cells: a higher expression in the Wnt3a-contacting cell indicates maintenance of a naïve ESC, whereas a lower expression in the Wnt3a-distal cell indicates a shift towards a more differentiated state.

To analyse ACD in WT or Wnt/β-catenin pathway KO ESCs, we seeded single cells at low density in the presence of Wnt3a- or iWnt3a-beads for 6 hours prior to fixation. Then we analysed divided cell pairs where a bead is in clear contact with only one of the two daughter cells. This ensured that only cell pairs with an asymmetric presentation of the Wnt3a signal were analysed (**Fig. 9A**). We distinguished three categories: a “Proximal” doublet consisting of a cell contacting a Wnt3a-bead (Wnt3a-proximal) with higher pluripotency marker signal, and a Wnt3a-distal cell with reduced pluripotency marker expression. Conversely, a doublet where the farthest cell expresses more pluripotency marker was named a “Distal” doublet. An even distribution, with no significant bias to either cell, was named “Distributed”. Of these, only the “Proximal” condition represents a Wnt3a-mediated ACD.

When contacting a Wnt3a-bead, most WT ESC doublets have “Proximal” marker expression and have therefore undergone Wnt3a-mediated ACD (**Fig. 9B-D**). On the other hand, the majority of WT ESCs dividing with iWnt3a-beads are “Distributed”, with a similar partitioning of pluripotency markers between daughter cells. While Lrp5KO ESCs have a reduced ability to precisely align the spindle towards a Wnt3a signal (**Fig. 8E and F)**, their capacity for Wnt3a-mediated ACD is retained (**Fig. 9B-D**). ESCs lacking Lrp6 or β-catenin (Lrp6KO,

Lrp5/6dKO, βKO) however, show impaired ACD (**Fig. 9B-D**), with cell pairs predominantly having "Distributed" expression of Nanog, Rex1 and Sox2 between daughter cells (**Fig. 9B-D**).

To validate the roles of Lrp6 and Lrp5, we transiently transfected Lrp5/6dKO ESCs with a plasmid encoding GFP and the *Lrp6* sequence and sorted them into GFP^+ (Lrp5KO, Lrp6 overexpression*, OE*) and GFP^- (Lrp5/6dKO) populations (**Fig. 10A and B**). Lrp5/6dKO cells overexpressing Lrp6 (GFP^+) could not efficiently align the spindle towards the Wnt3a-bead during mitosis (**Fig. 10C**). However, Wnt3a-oriented ACD was rescued in these cells, as shown by an increased rate of "Proximal" doublets, quantified for Sox2 and Nanog (**Fig. 10D-F**). Altogether, these results reiterate differences between Lrp5 and Lrp6 in the regulation of spindle orientation and ACD.

Considering all evidence, we have shown that the co-receptor Lrp6 and β-catenin play co-dependent roles in the positioning of localized Wnt3a signals at the membrane of ESCs, as well as in regulating spindle orientation and ensuring asymmetric partitioning of cell fate between the daughter cells. KO of these components in ESCs results in severely impaired activation of the Wnt/β-catenin pathway, as well as impaired recruitment of Wnt3a-beads. Lrp5KO ESCs retain higher capacity to activate the Wnt/β-catenin pathway in response to solubilized Wnt3a, to recruit Wnt3a beads and to induce ACD, despite a compromised spindle orientation towards the Wnt3a-bead. Importantly, regardless of clonal variability observed in the initial interaction stages between the cells and the Wnt3a signals, the downstream phenotypes observed are strongly retained when the cells divide.

AMPA-type iGluRs participate in controlling Wnt3a-oriented ACD

Our data has shown that AMPA/Kainate receptors activity is required for Wnt3a signal recruitment and interaction dynamics in ESCs, suggesting a pervasive crosstalk with the Wnt/β-catenin pathway activity. Next, we explored whether such effects span beyond early Wnt3a-stem cell interaction in modulating the process of division.

Wnt3a-beads fail to orient the spindle of AMPA/Kainate receptor-defective ESCs. GriK1/3dKO, GriA3/4dKO and WT ESCs treated with CNQX show misoriented spindle distributions (**Fig. 11A**). In Kainate-receptor KO cells, spindle orientation angles accumulate between 0°-60°, while GriA3/4dKO ESCs or CNQX-treated cells present broader, randomised spindle angle distributions (Chi-squared test, $P>0.05$). All AMPA/Kainate-type iGluR-defective cells are significantly different to the Wnt3a-biased spindle orientation observed in WT ESCs (K-S statistical tests, **Fig. 11A**).

Post-division doublet analysis revealed that, while GriK1/3dKO ESCs largely exhibit Wnt3a-oriented ACD, GriA3/4dKO or CNQX treatment reduces the proportion of “Proximal” doublets dividing cells (**Fig. 11C-E**).

To confirm these results we treated WT ESCs with NBQX, a pharmacological inhibitor specific to AMPA-receptors (Goldstein and Litwin, 1993). When compared to control ESCs treated with DMSO, NBQX-treated cells also fail to orientate the spindle towards a Wnt3a-bead (**Fig. 11B**) or undergo Wnt3a-oriented ACD (**Fig. 11F-H**).

Our data indicate that AMPA/Kainate-type iGluR activity has important roles throughout the interaction between ESCs and localized sources of Wnt3a. GriK1/3dKO impairs Wnt3a-bead recruitment without affecting the number or length of the cytonemes, or the rate of cytoneme generation in the population. AMPA-type receptors (involving GriA3/4) play lesser roles in ensuring Wnt3a-bead recruitment. Yet, both AMPA and Kainate iGluRs are important to correctly position the bead at the cell membrane, and to align the mitotic spindle towards the Wnt3a signal. Nevertheless, precise spindle orientation is also not required for Wnt3a-oriented ACD in these cells: Kainate receptors are dispensable for ACD but lack of GriA3/4 leads to reduced asymmetric cell fate marker segregation.

Together with our analysis of Wnt/β-catenin pathway KO ESCs, our results suggests that a dynamic crosstalk between AMPA/Kainate-receptor signalling and Lrp6 is not only involved in signal recognition and response, as previously shown, but is important to regulate the spatial organisation and specification of dividing ESCs by Wnt3a.

DISCUSSION

Cell fate and spatial positioning occur in concert to achieve proper tissue organization. In the stem cell niche, responsive stem cells receive Wnts as a cue for self-renewal (Clevers et al., 2014; Garcin and Habib, 2017). In a spatial context, Wnt reception has been shown to induce cell polarization and asymmetric cell division (ACD), in an evolutionarily conserved manner (Goldstein et al., 2006; Huang and Niehrs, 2014; Mizumoto and Sawa, 2007; Ouspenskaia et al., 2016; Sugioka et al., 2011; Walston et al., 2004).

Understanding initial ligand recruitment to stem cell membranes may benefit regenerative medicine and the targeting of Wnt-related diseases. However, the study of dynamic, localized Wnt reception by single stem cells is impeded by difficulties in visualising secreted Wnts. The Wnt3a-bead (Habib et al., 2013; Lowndes et al., 2017) allows a temporal analysis spanning the entire duration of the stem cell—Wnt3a-bead interaction: from cell morpho-motility prior to contact and initial bead recruitment by cytonemes, to the dynamic interaction at the cell membrane, ultimately leading to effects on spindle orientation and ACD.

AMPA/Kainate-type iGluR activity, and its crosstalk with the Wnt/β-catenin pathway, controls cytoneme-mediated recruitment of Wnt signals in mouse embryonic stem cells (ESCs) (Junyent et al., 2020)**.** Additionally**,** components of the Wnt pathway regulate the length and number of cytonemes (Junyent et al., 2020). Conversely, we show in this study that knockout of AMPA- or Kainate-receptors does not affect cytoneme formation.

The Wnt co-receptors Lrp5 and Lrp6 have mostly been studied in the context of β-catenin–dependent signalling, where they have overlapping functions (He et al., 2004; Houston and Wylie, 2002; Kelly et al., 2004; Tamai et al., 2000; Wehrli et al., 2000), albeit to different levels of efficiency (Holmen et al., 2002; MacDonald et al., 2011). Here, we demonstrate differing roles between them: endogenous expression of Lrp6 alone in ESCs (in Lrp5KO) results in an increased rate of cytoneme formation over WT ESCs, while cells lacking Lrp6 (Lrp6KO and Lrp5/6dKO) have a reduced rate of cytoneme formation, suggesting a distinct role for Lrp6 in cytoskeleton regulation.

Both Lrp5 and Lrp6 contain cytoplasmic domains that can bind to regulators of actin filaments (Brown et al., 1998; Krause et al., 2003; Lian et al., 2016; Zhu et al., 2012), however this region of Lrp5 has just 37% identity to Lrp6, compared to 69% overall sequence identity between them (MacDonald et al., 2011). We speculate that such differences might contribute to their differential roles in cytoneme formation/elongation: Lrp5 may compete with Lrp6 for the interaction of Wnt-pathway components or cytoskeletal regulators. Hence, improved Lrp6-cytoskeleton interactions may facilitate the increased rate of cytoneme formation and initial Wnt3a-bead recruitment observed in Lrp5KO ESCs.

WT ESCs use cytonemes to efficiently recruit Wnt3a-beads, and subsequently position them near the centre of the cell. iWnt3a-beads cannot be recruited with the same efficiency. Additionally, iWnt3a-beads are maintained nearer the periphery of the cell, with shorter and less stable interactions. AMPA/Kainate-receptor activity is involved throughout the Wnt3a-interaction. AMPA- or Kainate-receptor knockout (KO) ESCs, similarly to those lacking Lrp6 or β-catenin, are able to recruit Wnt3a-beads via cytonemes, but over 12 hours are inefficient in their population-wide accumulation of Wnt3a-signal compared to WT or Lrp5KO ESCs.

Beyond the initial interaction between cell and Wnt3a-ligand, a role for AMPA/Kainate-receptors lies in controlling the dynamics of Wnt3a on the membrane. Unlike WT ESCs, neither AMPA- nor Kainate-receptor KO cells are able to relocate the Wnt3a-bead from the cytoneme-periphery and retain it near the centre of the cell. Pharmacological inhibition of both AMPA- and Kainate-receptors together by CNQX resulted in a similar phenotype with an enhanced effect. The KO of Wnt-pathway components Lrp5, Lrp6 or β-catenin also reduces the ability to position a Wnt3a-bead on the membrane near the centre of the cell.

Following ligand-receptor binding, Wnt-pathway component polarization (Capelluto et al., 2002) and oligomerization (Cong et al., 2004) are suggested to play roles in the enhancement or modulation of Wnt signalling (Bilic et al., 2007). Here, the spatial stabilization and colocalization of upstream and downstream pathway components at a 'signalling hub' may be critical for efficient signal transmission. In fact, we previously demonstrated colocalization of Lrp6 and AMPA/Kainate-receptors during ESC interaction with a Wnt3a-bead (Junyent et al., 2021).

Membrane receptors, including glutamate receptors (Yang et al., 2006), have been demonstrated to flow from membrane protrusions towards the centre of the cell. This motion can be promoted by directed movement of the actin cytoskeleton (Hanley, 2014; Yu et al., 2010) and its efficiency can be governed by the activation of the pathway (Hartman et al., 2009). Areas of relative membrane concavity, such as the cell centre away from the periphery, have also been shown to enhance membrane receptor interactions with intracellular components (Rangamani et al., 2013). This process may be required for more efficient signalling (Schmick and Bastiaens, 2014). Therefore, the control of the Wnt3a-bead positioning in WT ESCs may facilitate efficient protein interactions required for signal transduction, enhancing downstream pathway activation.

After Wnt3a-bead recruitment and upon progression to mitosis, WT ESCs orientate the spindle towards the source of localized Wnt3a at anaphase. Perturbation of the AMPA/Kainate-receptors or Wnt/β-catenin pathway components resulted in significant

impairment of the alignment of the spindle to localized Wnt3a, suggesting that both pathways function in concert during this process.

Interestingly, AMPA-receptors are involved in Wnt3a-mediated ACD. While Kainate-receptor KO had no significant effect, both AMPA-receptor KO and AMPA-receptor–specific inhibition by NBQX significantly compromised Wnt3a-mediated ACD. Similarly, Wnt3a-mediated ACD is impaired when ESCs lack Lrp6 or β-catenin. Lrp5KO ESCs, however, much like with Kainate-receptor KO, remain able to asymmetrically segregate pluripotency markers to the proximal cell, despite the lack of precise alignment of the spindle towards a Wnt3a-bead at anaphase. Therefore, a robust spindle orientation towards a Wnt3a-bead is not required for asymmetric fate outcome. Our data further demonstrates a differential requirement for Lrp5 and Lrp6 in ESCs, beyond the rate of cytoneme formation, in the regulation of cell fate. Interestingly, the *Drosophila* neuroblast can tolerate certain degrees of spindle misorientation due to disruption in internal polarity cues during early stages of cell division. These cells can overcome initial misorientation and retain the prospective cell fate of the daughter cells (Knoblich et al., 1995; Peng et al., 2000; Schober et al., 1999).

In summary, response to localized Wnt3a reception and the downstream Wnt3a-mediated ACD is not orchestrated by the Wnt/β-catenin pathway alone, but also by crosstalk with AMPA/Kainate-type glutamate-receptor activity.

Glutamate-receptor activity is an evolutionarily conserved pathway that links homologous proteins in prokaryotes (*e.g.* GluR0 (Chen et al., 1999)) and plants (GLRs (Forde and Roberts, 2014; Ortiz-Ramírez et al., 2017)) with metazoans (iGluRs). In mammals, they are well known for their function in excitatory synaptic signalling (Niciu et al., 2012). However, there is a more ancient role for glutamate signalling that pervades throughout single- and multi-cellular organisms alike: chemotaxis.

From non-neuronal mammalian cells (Gupta and Chattopadhyay, 2009), to plant reproductive cells (Ortiz-Ramírez et al., 2017) and bacteria (Brumley et al., 2019), sensitivity to glutamate or related molecules can provide a spatial signal that influences cellular organisation. In *E. coli*, cytoplasmic proteins are segregated to the cellular poles by interaction and colocalization with glutamate-sensitive chemoreceptors (Maddock and Shapiro, 1993). This therefore presents a glutamate-receptor–mediated mechanism for the spatial orientation of intracellular components in response to external signals. Further, glutamate acts as a nutrient (Hottes et al., 2004) and chemoattractant (Felzenberg et al., 1996) to the bacterium *Caulobacter crescentus.* This bacterium undergoes ACD to replicate its ‘stalked’ form, and to generate a motile ‘swarmer’ cell. Crucially, in *C. cresentus*, chemoreceptors are synthesized in the pre-divisional cell (Gomes and Shapiro, 1984),

before being asymmetrically polarized at division to the pole of the cell along with other protein components of the swarmer cell fate (Alley et al., 1992) . It remains to be determined whether the glutamate-sensing machinery is specifically required for the ACD of *C. cresentus* and other bacteria. However, these findings above suggest an evolutionarily conserved link between the sensing of external chemo-attractants such as glutamate, and the polarization and compartmentalisation of cell fate components.

As this ancient function for glutamate-receptor activity is present in ESCs during Wnt3a-mediated ACD, it may prove to be a mechanism that influences stem cell biology, cell fate and tissue organisation throughout mammalian adult stem cells and metazoans.

MATERIALS AND METHODS

Cell culture

Wild-type W4 (129S6/SvEvTac) mouse ESCs or ESCs knock-out for Lrp5, Lrp6 or Lrp5/6dKO (generated as described in (Junyent et al., 2020)) were maintained in ESC basal media containing Advanced DMEM/F12 (cat. num. 12634028, ThermoFisher), 10% ESC-qualified foetal bovine serum (FBS, cat. num. ES-009-B, Millipore), 1% penicillin-streptomycin (cat. num. P4333, Sigma), 2 mM GlutaMax (cat. num. 35050061, ThermoFisher), 50 µM β-mercaptoethanol (cat. num. 21985-023, ThermoFisher) and 1000 U/mL recombinant Leukaemia Inhibitory Factor (LIF; cat. num. 130-095-775, Miltenyi), supplemented with with 2i: MEK inhibitor PD0325901 (1 µM, cat. num. 130-104-170, Miltenyi) and GSK3 inhibitor CHIR99021 (3 µM, cat. num. 130-104-172, Miltenyi). Heterozygous β-catenin deficient ($\beta^{fl/-}$) ESCs, with an inducible flox β-catenin, and stably carrying a Cre-ER-T2 cassette under the control of a chicken β-actin promoter (generated in a W4 129S6/SvEvTac background by (Raggioli et al., 2014)) were cultured in the same conditions. Media was changed daily, and cells were grown at low density until formation of mid-sized colonies before passaging (every 3-4 days). To passage ESCs, colonies were rinsed with PBS, treated with 0.25% trypsin-EDTA (T-E, cat. num. 25200056, ThermoFisher) for 4 min at 37°C, 5%CO_2, resuspended using ESC basal media and centrifuged at 1200 x *g* for 4 minutes. Pelleted cells were resuspended in ESC basal media, counted and seeded in a clean tissue culture-treated 6-well plate at low density (~7,000 cells/well) in complete ESC media (containing LIF and 2i). In some experiments, 24 hours before use, 2i was withdrawn and replaced with soluble Wnt3a protein (200 ng/mL).

β-catenin knock-out in $\beta^{fl/-}$ cells was induced through the addition of 0.1 µg/mL 4-hydroxy-tamoxifen (4-HT, cat. num. H6278, Sigma) to the media every 24 hours for 72 hours. Cells treated for 3 days with 4-HT were used in the experiments (referred to as βKO in the text).

All cell lines were maintained at 37°C, 5%CO_2 and were routinely tested for mycoplasma infection.

Pharmacological inhibition of iGluRs

When indicated in the text, figures or figure legends, cells were treated with the AMPA/Kainate iGluR inhibitor cyanquixaline (CNQX, 10 µg/mL, cat. num. C127, Sigma) or the AMPA-iGluR specific inhibitor 2,3-dioxo-6-nitro-7-sulfamoyl-benzo[f]quinoxaline (NBQX, cat. num. 373, Tocris). Drugs were dissolved in ESC complete media (no 2i) to the desired concentration and were added to the cells at the beginning of the experiment. For Wnt/β-

catenin pathway activation experiments, CNQX was added to the cells 1h before solubilized Wnt3a or Wnt3a-bead addition.

Generation of KO ESCs by CRISPR/Cas9-mediated gene editing

Generation of KO ESCs was achieved by CRISPR/Cas9-mediated gene editing, following (Ran et al., 2013). gRNA sequences adjacent to a protospacer adjacent motif (PAM) and targeted at an early conserved exon in *Lrp5, Lrp6*, *GriA3*, *GriA4*, *GriK1* and *GriK3* were designed in Geneious 11 (Biomatters). gRNAs were scored for on- and off-target effects against the whole mouse genome, and sequences with low off-target score were synthetised as oligonucleotides and cloned into a PX458 plasmid (Addgene plasmid #48138). gRNA sequences used can be found in **Fig. 1 – Figure Supplement 1** and **Fig. 5 – Figure Supplement 1**.

WT (to generate KO for *Lrp5*, *Lrp6*, *GriA3* and *GriK3*), Lrp6KO (to generate the Lrp5/6dKO line), GriA3KO (to generate GriA3/4dKO cells) or GriK3KO (to generate GriK1/3dKO) ESCs were transfected with 1 µg PX458 plasmid containing the sequence for the correct gRNA, using JetPrime (cat. num. 114-07, Polyplus transfection) according to manufacturer instructions. After 24h, transfected cells were sorted (as described in the “Fluorescence activated Cell Sorting” section), and single GFP+ cells were collected in the wells of a 96-well tissue culture-treated plate, in ESC complete media with LIF and 2i. Individual clones were grown until formation of colonies, then expanded by passaging twice. Genomic DNA was extracted using a DNeasy Blood and Tissue extraction kit (cat. num. 69506, Qiagen) and the targeted region was amplified by *Taq* polymerase PCR (cat. num. M7501, Promega). Sequence verification was achieved by TOPO-cloning (cat. num. 450159, ThermoFisher) of the *Taq*-PCR fragments, transformation into Top10 chemically competent bacteria (cat. num. C404006, ThermoFisher) and clonal selection. At least 12 TOPO-clones per mutant clone were analysed by Sanger sequencing (Source Bioscience). Clonal ESC lines with homozygous mutations that generated a frame-shift mutation inducing a premature stop codon were selected for the experiments. KO ESCs were cultured as described above.

Preparation of Wnt3a-microbeads

Recombinant Wnt3a proteins were produced as described before (Habib et al., 2013; Junyent et al., 2020), or purchased (cat. num. 1324-WN, R&D systems). Wnt3a proteins were immobilized to 2.8 µm carboxylic acid–coated Dynabeads® (cat. num. 14305D, ThermoFisher), as described before (Habib et al., 2013; Junyent et al., 2020; Lowndes et al., 2017). Briefly, the carboxylic acid groups on the Dynabeads® were activated by a 30-minute incubation with N-(3-Dimethylaminopropyl)-N′-ethylcarbodiimide (EDC, cat. num. 39391, Sigma) and N-Hydroxysuccinimide (NHS, cat. num. 56480-25G, Sigma). 50 mg/mL EDC

and NHS solutions were prepared in 25 mM cold 2-(N-morpholino) ethanesulfonic acid (MES, cat. num. M3671-50G, Sigma), at pH5. EDC/NHS incubation was performed in constant rotation at room temperature (RT). Following activation, beads were retained using a magnet and washed three times with 25 mM MES buffer (pH 5). Solubilized Wnt3a protein (500 ng) was diluted 1:5 in MES buffer (pH 5) and incubated with the beads for 1 hour in constant rotation, at RT. Beads were washed again three times with PBS (pH 7.4) before storage in media containing 10% FBS at 4°C. Inactivation of Wnt3a beads was achieved through incubation with 20 mM Dithiothreitol (DTT; Life Technologies, #P2325) for 30 minutes at 37°C. Following incubation with DTT, beads were washed three times in PBS before storage in media containing 10% FBS at 4°C (up to 10 days). Before use in the experiments, Wnt3a-bead activity was validated as described before (Habib et al., 2013; Junyent et al., 2020; Lowndes et al., 2017).

Time-course live-cell imaging

To analyse the dynamics of ESCs and Wnt3a-bead interaction, 2,500 ESCs/well mixed with 0.3 µg Wnt3a-beads/well were seeded in a tissue culture-treated, clear-bottomed, black-walled 96-well plate (cat. num. 3603, Corning) in complete media containing LIF (no 2i). Cells and beads were allowed to settle at 37°C, 5% CO_2 for 30 min. Then, the plate was placed in a Zeiss inverted Axio Imager epifluorescence microscope, equipped with a CoolSNAP HQ2 CCD camera. Between 20-30 positions containing cells and beads were selected and cells were imaged using a 10x/0.3 dry objective, for brightfield, every 1 minute for 12 hours. The Zen 2 (Blue edition, Zeiss) software was used for acquisition. The resulting videos were analysed in Fiji (ImageJ) as described in the next sections. Three or more independent videos were generated for each cell line or condition (detailed in the figure legends and the source data files).

To image the dynamics of the cytonemes in ESCs, 5,000 ESCs were seeded in a well of an ibiTreat-modified µ-Slide 8 well slide (cat. num. 80826, Ibidi) in ESC complete media with LIF (no 2i). Cells were incubated at 37°C, 5% CO_2 for 4h to allow cell attachment and cytoneme generation. Cells were stained with CellMask Deep Red plasma membrane stain (1x concentration, cat. num. C10046, ThermoFisher) for 15 min at 37°C, 5%CO_2. Cells were then rinsed once with ESC complete media and imaged immediately in a Nikon Eclipse Ti Inverted Spinning Disk confocal (equipped with a Yokogawa CSU-1 disk head and an Andor Neo sCMOS camera, and an incubation system at 37°C, 5% CO_2). Cells were imaged using a Plan Apo lambda 40x/0.95 dry objective every 10 seconds, for 10 minutes. The resulting videos were processed in Fiji (ImageJ) and presented in inverted grayscale.

Image analysis: Number and length of the cytonemes in ESCs

Brightfield time-course videos (at 1 min resolution) were used to measure the average number and maximum length of the cytonemes in WT, GriK1/3dKO and GriA3/4dKO ESCs. Cells from each condition that attach and generate cytonemes were selected. For each cell, the number and length of their cytonemes was measured from the cell centre, 10 times in timepoints separated by 10 minutes. The distance between the cell centre and the membrane was also measured in these timepoints. The average number of cytonemes, as well as the maximum length for any cytoneme was calculated, and the average cell centre to cell membrane distance was subtracted from the values. The normalized values were reported in the figure.

Image analysis: Percentage of cells with cytonemes or Wnt3a-beads over time

Brightfield videos of ESCs and Wnt3a-beads at 1 min resolution were also used to measure the percentage of cells presenting cytonemes or contacting Wnt3a-beads. Cytoneme generation was analysed every hour for the first 4 hours of each video (timepoints 0h to 4h), while Wnt3a-bead contact was analysed for the totality of the video (timepoints 0h to 12h). Several positions were analysed for each independent video, on Fiji (ImageJ), to count the total number of cells in the frame, the number of cells with cytonemes and/or the number of cells in contact with Wnt3a-beads. Cell counts in the different positions of each video were summed to avoid position-specific differences, and the percentage values were calculated per time-point, as presented in the figures.

Image analysis: Wnt3a-bead position and movement in the cell and cell movement

Single ESCs that recruited a Wnt3a-bead with a cytoneme and retained contact with it for ≥ 180 min were selected to measure Wnt3a-bead position and movement on the membrane. The same cells were used to measure cell movement. For each cell and each minute, the position of the cell centre, the Wnt3a-bead and the membrane were registered as X and Y coordinates using the “Manual tracking” plugin on Fiji (ImageJ).

First, the distances between the cell centre and the Wnt3a-bead ($\text{Distance}_{\text{cell-bead}}$) or the cell centre and the membrane ($\text{Distance}_{\text{cell-membrane}}$, cell radius) were calculated for each minute as:

$$Distance_{cell-bead} = \sqrt{(}(x_{bead} - x_{cell})^2 + (y_{bead} - y_{cell})^2)$$

$$Distance_{cell-membrane} = \sqrt{(}(x_{membrane} - x_{cell})^2 + (y_{membrane} - y_{cell})^2)$$

Then, the ratio between the $\text{Distance}_{\text{cell-bead}}$ and the $\text{Distance}_{\text{cell-membrane}}$ (cell radius) was calculated and reported in the figure.

Second, cell movement was calculated as mean squared displacement (MSD), based on the position of the cell centre (P_{cell}) over the 180 min analysed, as:

$$MSD_{cell}(\tau) = \langle \Delta P_{cell}(\tau) \rangle = \langle [P_{cell}(t+\tau) - P_{cell}(t)]^2 \rangle$$

Where τ is the interval of time between two positions (1 min).

Finally, the normalized position of the Wnt3a-bead relative to the position of the cell (Normalized $position_{bead}$, NP_{bead}) was calculated for each time point (t) as:

$$Normalized\ position_{bead}(t) = NP_{bead}(t) = (x_{bead}(t) - x_{cell}(t)\ , y_{bead}\ (t) - y_{cell}(t))$$

In this way, the movement of the Wnt3a-bead was normalized to the movement of the cell. Then, the MSD of the Wnt3a-bead was calculated with $\tau = 1\ minute$ as:

$$MSD_{bead}(\tau) = \langle \Delta NP_{bead}(\tau) \rangle = \langle [NP_{bead}(t+\tau) - NP_{bead}(t)]^2 \rangle$$

Image analysis: Percentage of bead retention/dropping

Brightfield videos of ESCs at 1 min resolution were also used to measure the percentage of cells that retain or drop the Wnt3a-bead after recruitment. A sample of cells from each condition were observed, and the time of Wnt3a-bead uptake with a cytoneme was registered (t_{uptake}). Then, the cell was observed for a further 180 min ($t_{uptake+180}$): if a cell lost contact with the Wnt3a-bead before $t_{uptake+180}$, the cell was qualified as “drops”; if contact was maintained beyond $t_{uptake+180}$, the cell was qualified as “retains”. Cells that divided within the observed period were excluded from the analysis. The percentage of cells that drop or retain Wnt3a-beads over the total number of cells analysed was presented in the figures.

Image analysis: Spindle orientation

The videos at 1 min resolution were also used to measure spindle orientation. Cells dividing in contact with a Wnt3a-bead were analysed. The “Angle” tool in Fiji (ImageJ) was used to measure the angle between the minor axis and the Wnt3a-bead position at anaphase for all conditions (**Fig. 8, 10 and Movie 9**). Rose-plots were generated with a custom Python script.

Immunofluorescence and measurement of asymmetric cell division

3,000 ESCs/well mixed with 0.3 µg Wnt3a-beads/well were seeded onto human fibronectin (10 µg/mL, cat. um. 7340101, VWR/SLS) coated 8-well slides (cat. num. 80828, Thistle Scientific) in ESC complete media containing LIF (no 2i). Slides were incubated for 6h at 37°C, 5% CO_2. After incubation, media was gently aspirated, and cells were fixed with 4% paraformaldehyde for 8 min at RT. Cells were then washed 3 times in staining buffer (PBS with 0.1% Bovine Serum Albumin (cat. num. A8806, Sigma), 0.05% NaN_3 (cat. num. S2002,

Sigma) and 0.001% Tween20 (cat. num. P2287, Sigma)) for 5 minutes each. Slides were incubated in primary antibody diluted in staining buffer at 4°C overnight. Then, slides were carefully washed 3 times for 5 minutes in staining buffer and incubated with AlexaFluor (AF)-conjugated secondary antibodies diluted in staining buffer, for 1h at RT. Final washes were performed with staining buffer containing DAPI (cat. num. D1306, ThermoFisher) at 1:1000 dilution. Slides were carefully mounted with ProLong Gold antifade mounting media (cat. num. P10144, Life Technologies) and let to solidify for 24-48h before imaging.

Slides were imaged on a Zeiss inverted Axio Imager epifluorescence microscope using Zen 2 (Blue edition, Zeiss) software and equipped with a CoolSNAP HQ2 CCD camera. A 40x/1.3 oil immersion objective was used. Z-stacks were taken according to the optimal interval. Images were processed, deconvolved, and quantified using Volocity software (Perkin Elmer) or analysed in Fiji (ImageJ).

Quantification involved reconstruction of the cell based on “Sum” projection and manual identification of divided cells. Cells were qualified as “Proximal”, “Distributed” or “Distal” by three independent researchers according to the partitioning of Nanog, Rex1 or Sox2 intensities between the Wnt3a-bead-proximal and -distal cell. Additionally, samples of doublets were allocated by semi-automated 3D intensity quantification in the Wnt3a-bead proximal and -distal cell using Volocity (Perkin Elmer) or Fiji (ImageJ). In these cases, mean fluorescent intensity in the proximal and distal cells was measured for each channel and normalized to background intensity. The percentage of protein partitioning in the proximal or distal cell was used to allocate doublets as follows: “Proximal”, >55% of protein in bead-proximal cell; “Distributed”, 55% to 45% of protein in bead-proximal cell; “Distal”, <45% of protein in bead-proximal cell.

Antibodies

The antibodies (Ab) used in this study were anti-Nanog (monoclonal rat Ab, clone eBioMLC-51; 1:500, cat. num. 14-5761-80, ThermoFisher), anti-Rex1 (rabbit polyclonal Ab, 14HCLC; 1:1500, cat. num. 710190, ThermoFisher), anti-Rex1 (rabbit polyclonal Ab; 1:500, cat. num. ab28141, Abcam), anti-Sox2 (mouse monoclonal Ab, clone 245610; 1:500, cat. num. MAB2018, R&D systems) and AF488-, AF555- and AF647-tagged secondary antibodies (donkey; 1:1000, cat. num. A-21208, A-31572, A-31571, ThermoFisher).

Fluorescence Activated Cell Sorting

Fluorescence activated cell sorting (FACS) was employed to detect Wnt3a response in WT, KO or CNQX-treated ESCs stably expressing 7xTCF-eGFP//SV40-mCherry (Junyent et al., 2020). Following incubation with control media (ESC basal media), media containing

solubilised Wnt3a (200 ng/mL), or addition of a high density of Wnt3a- or iWnt3a-beads (6.25 µg/cm^2) for 24h, cells were harvested using 0.25% T-E, filtered and analyzed using a FACSFortessa system (BD Biosciences). The gating strategy included gating for SSC-FSC (cells), SSC-A-SSC-W (single cells), SSC-DAPI (alive cells), SSC-PE Texas Red (mCherry+ cells), and SSC-FITC (eGFP). GFP+/- gate was established using CNTRL-treated and Wnt3a-treated WT ESCs. Analysis was performed using the FlowJo software (FlowJo).

FACS was also used to purify GFP+ and GFP- populations from an Lrp5/6dKO ESC line transfected with pEGFP-Lrp6 (Habib et al., 2013), or to sort single GFP+ cells transfected with PX458 CRISPR/Cas9 plasmids. Cells were transfected with 1 µg pEGFP-Lrp6 or PX458 using JetPrime, 24h before sorting. Then, a cell suspension was prepared as described before, and cells were sorted using a FACSAriaII system (BD technologies). The gating strategy included gates for cells, single cells, alive cells and GFP (as described before), but laser intensities were adjusted as required. GFP+/- gates were established using control (non-transfected) ESCs and cells transfected with the plasmids. For pEGFP-Lrp6 sorting, only Lrp5/6dKO ESCs transfected with the plasmid were used for sorting GFP$^-$ and GFP$^+$ cells. Sorted cells were collected in complete ESC media containing LIF (no 2i), counted and seeded for experiments (as described before). For PX458 sorting, single cells were sorted in tissue culture-treated 96-well plates in ESC complete media (with LIF and 2i).

Quantitative PCR

Quantitative PCR (qPCR) was used to measure *Axin2* expression in response to Wnt/β-catenin pathway stimulation. 2.0 x 10^4 WT or KO ESCs/well were seeded in a tissue culture-treated 12-well plate in ESC complete media supplemented with LIF (no 2i). Plates were incubated at 37°C, 5% CO_2 for 24h. Then, media was aspirated and replaced with ESC complete media (LIF, no 2i) with or without 200 ng/mL solubilized Wnt3a. Cells were returned to the incubator for 24h. Cell lysis, RNA extraction and purification was performed with an RNeasy mini kit (cat. num. 74106, Qiagen), following manufacturer instructions. 500 ng RNA were retrotranscribed with a QuantiTect reverse transcription kit (cat. num. 205313, Qiagen) following manufacturer instructions. qPCR was prepared with 2x TaqMan Fast Universal PCR MasterMix (cat. num. 4366072, ThermoFisher) and TaqMan probes for *Axin2* (Mm00443610_m1, cat. num. 4331182, ThermoFisher) and GAPDH (Mm99999915_g1, cat. num. 4351370, ThermoFisher). qPCR was performed in a Bio-Rad CFX384 system (Bio-Rad). The threshold-cycle values (Ct) of *Axin2* were normalized first to Ct values of GAPDH (DCt), and then to the average DCt values of the WT CNTRL condition (DDCt) and were reported as 2^{-DDCt} in the figures.

Statistical analysis

Data representation and statistical analysis were performed using Prism (GraphPad), as described in the figures. ANOVA (one- or two-way) analysis, followed by Tukey's, Dunnett's or Šídák's multiple comparisons test was performed to compare data between conditions. For analysis of spindle orientation, the Kolmogorov-Smirnov statistical test was performed to compare between conditions of non-normally distributed data and Chi-square analysis was performed to compare between observed data and the expected/randomized distribution. The statistical analysis used for each assay is described in the figure legends. In all experiments, biological replicates (n) for each assay comprise of experiments performed independently from one another, and as such are from different cultured populations/passages of cells, different sessions of imaging/measurement, and independent media/reagent/cell dilution. Sample sizes (N) were selected such that the power of the statistical analysis performed was sufficient, in accordance with previous studies (Habib et al., 2013; Junyent et al., 2020). When indicated in the figure legends, the cells analysed were pooled approximately evenly from at least three independent experiments, and analysis were performed on the pooled data. Outliers were considered as individual data points significantly outside the range of possible/meaningful values for each assay and were excluded from subsequent analysis. For all figures, symbols indicate statistical significance as follows: $*p < 0.05$, $**p < 0.01$, $***p < 0.001$, $****p < 0.0001$. Non-significance was set as $p > 0.05$. All numerical source data, as well as statistical analysis results including adjusted *p*-values can be consulted in the source data file for each figure.

ACKNOWLEDGEMENTS

This work was supported by a Sir Henry Dale Fellowship (102513/Z/13/Z) to S.J.H.

CONTRIBUTION

S.J., J.R. and S.J.H. designed the study, performed experiments and analysed data, wrote the manuscript and prepared figures. J.L.A.S, C.L.G and T-J.T. performed experiments and analysed data. M.W. and J.L-B. analysed data. S.J.H, conceived the idea, led the project and provided financial support for the project.

COMPETING INTERESTS

No competing interests.

REFERENCES

Alley MRK, Maddock JR, Shapiro L. 1992. Polar localization of a bacterial chemoreceptor. *Genes Dev* **6**:825–836. doi:10.1101/gad.6.5.825

Bertrand V. 2016. B-Catenin-Driven Binary Cell Fate Decisions in Animal Development. *Wiley Interdiscip Rev Dev Biol* **5**:377–388. doi:10.1002/wdev.228

Bilic J, Huang Y-L, Davidson G, Zimmermann T, Cruciat C-M, Bienz M, Niehrs C. 2007. Wnt Induces LRP6 Signalosomes and Promotes Dishevelled-Dependent LRP6 Phosphorylation. *Science (80-)* **316**:1619–1622. doi:10.1126/science.1137065

Brorson JR, Li D, Suzuki T. 2004. Selective Expression of Heteromeric AMPA Receptors Driven by Flip-Flop Differences. *J Neurosci* **24**:3461–3470. doi:10.1523/JNEUROSCI.5023-03.2004

Brown SD, Twells RCJ, Hey PJ, Cox RD, Levy ER, Soderman AR, Metzker ML, Caskey CT, Todd JA, Hess JF. 1998. Isolation and characterization of LRP6, a novel member of the low density lipoprotein receptor gene family. *Biochem Biophys Res Commun* **248**:879–888. doi:10.1006/bbrc.1998.9061

Brumley DR, Carrara F, Hein AM, Yawata Y, Levin SA, Stocker R. 2019. Bacteria push the limits of chemotactic precision to navigate dynamic chemical gradients. *Proc Natl Acad Sci U S A* **166**:10792–10797. doi:10.1073/pnas.1816621116

Capelluto DGS, Kutateladze TG, Habas R, Finkielstein C V., He X, Overduin M. 2002. The DIX domain targets dishevelled to actin stress fibres and vesicular membranes. *Nature* **419**:726–729. doi:10.1038/nature01056

Chen GQ, Cul C, Mayer ML, Gouaux E. 1999. Functional characterization of a potassium-selective prokaryotic glutamate receptor. *Nature* **402**:817–821. doi:10.1038/45568

Clevers H, Loh KM, Nusse R. 2014. Stem cell signaling. An integral program for tissue renewal and regeneration: Wnt signaling and stem cell control. *Science* **346**:1248012. doi:10.1126/science.1248012

Cong F, Schweizer L, Varmus H. 2004. Wnt signals across the plasma membrane to activate the β-catenin pathway by forming oligomers containing its receptors, Frizzled and LRP. *Development* **131**:5103–5115. doi:10.1242/dev.01318

Cull-Candy S, Kelly L, Farrant M. 2006. Regulation of Ca2+-permeable AMPA receptors: synaptic plasticity and beyond. *Curr Opin Neurobiol* **16**:288–297. doi:10.1016/j.conb.2006.05.012

Felzenberg ER, Yang GA, Hagenzieker JG, Poindexter JS. 1996. Physiologic, morphologic and behavioral responses of perpetual cultures of Caulobacter crescentus to carbon, nitrogen and phosphorus limitations. *J Ind Microbiol Biotechnol* **17**:235–252. doi:10.1007/bf01574698

Forde BG, Roberts MR. 2014. Glutamate receptor-like channels in plants: A role as amino acid sensors in plant defence? *F1000Prime Rep* **6**:1–7. doi:10.12703/P6-37

Fuerer C, Nusse R. 2010. Lentiviral Vectors to Probe and Manipulate the Wnt Signaling Pathway. *PLoS One* **5**:e9370. doi:10.1371/journal.pone.0009370

Garcin CL, Habib SJ. 2017. A Comparative Perspective on Wnt / β -Catenin Signalling in Cell Fate Determination In: J.-P. Tassan JZK, editor. Asymmetric Cell Division in Development, Differentiation and Cancer, Results and Problems in Cell Differentiation 61, DOI 10.1007/978-3-319-53150-2_15. Springer International Publishing AG. pp. 323–350. doi:10.1007/978-3-319-53150-2

Genever PG, Maxfield SJ, Kennovin GD, Maltman J, Bowgen CJ, Raxworthy MJ, Skerry TM. 1999. Evidence for a novel glutamate-mediated signaling pathway in keratinocytes. *J Invest Dermatol* **112**:337–342. doi:10.1046/j.1523-1747.1999.00509.x

Goldstein B, Takeshita H, Mizumoto K, Sawa H. 2006. Wnt signals can function as positional cues in establishing cell polarity. *Dev Cell* **10**:391–6. doi:10.1016/j.devcel.2005.12.016

Goldstein JM, Litwin LC. 1993. NBQX is a selective non-NMDA receptor antagonist in rat hippocampal slice. *Mol Chem Neuropathol* **18**:145–152. doi:10.1007/BF03160028

Gomes SL, Shapiro L. 1984. Differential expression and positioning of chemotaxis methylation proteins in Caulobacter. *J Mol Biol* **178**:551–568. doi:10.1016/0022-2836(84)90238-9

Gupta R, Chattopadhyay D. 2009. Glutamate is the chemotaxis-inducing factor in placental extracts. *Amino Acids* **37**:271–277. doi:10.1007/s00726-008-0143-5

Habib SJ, Chen B-C, Tsai F-C, Anastassiadis K, Meyer T, Betzig E, Nusse R. 2013. A Localized Wnt Signal Orients Asymmetric Stem Cell Division in Vitro. *Science (80-)* **339**:1445–1448. doi:10.1126/science.1231077

Hanley JG. 2014. Actin-dependent mechanisms in AMPA receptor trafficking. *Front Cell Neurosci* **8**:1–8. doi:10.3389/fncel.2014.00381

Hartman NC, Nye JA, Groves JT. 2009. Cluster size regulates protein sorting in the immunological synapse. *Proc Natl Acad Sci U S A* **106**:12729–12734. doi:10.1073/pnas.0902621106

He X, Semenov M, Tamai K, Zeng X. 2004. LDL receptor-related proteins 5 and 6 in Wnt/β-catenin signaling: Arrows point the way. *Development* **131**:1663–1677. doi:10.1242/dev.01117

Hernandez AR, Klein AM, Kirschner MW. 2012. Kinetic Responses of -Catenin Specify the Sites of Wnt Control. *Science (80-)* **338**:1337–1340. doi:10.1126/science.1228734

Holmen SL, Salic A, Zylstra CR, Kirschner MW, Williams BO. 2002. A novel set of Wnt-Frizzled fusion proteins identifies receptor components that activate β-catenin-dependent signaling. *J Biol Chem* **277**:34727–34735. doi:10.1074/jbc.M204989200

Hottes AK, Meewan M, Yang D, Arana N, Romero P, McAdams HH, Stephens C. 2004. Transcriptional profiling of Caulobacter crescentus during growth on complex and minimal media. *J Bacteriol* **186**:1448–61. doi:10.1128/jb.186.5.1448-1461.2004

Houston DW, Wylie C. 2002. Cloning and expression of Xenopus Lrp5 and Lrp6 genes. *Mech Dev* **117**:337–342. doi:10.1016/S0925-4773(02)00205-8

Huang H, Liu S, Kornberg TB. 2019. Glutamate signaling at cytoneme synapses. *Science (80-)* **363**:948–955. doi:10.1126/science.aat5053

Huang YL, Niehrs C. 2014. Polarized Wnt signaling regulates ectodermal cell fate in Xenopus. *Dev Cell* **29**:250–257. doi:10.1016/j.devcel.2014.03.015

Junyent S, Garcin CL, Szczerkowski JLA, Trieu T-J, Reeves J, Habib SJ. 2020. Specialized cytonemes induce self-organization of stem cells. *Proc Natl Acad Sci* **117**:7236–7244. doi:10.1073/pnas.1920837117

Junyent S, Reeves J, Gentleman E, Habib SJ. 2021. Pluripotency state regulates cytoneme selectivity and self-organization of embryonic stem cells. *J Cell Biol* **220**. doi:10.1083/jcb.202005095

Kaur S, Mélénec P, Murgan S, Bordet G, Recouvreux P, Lenne P-F, Bertrand V. 2020. Wnt ligands regulate the asymmetric divisions of neuronal progenitors in C. elegans embryos . *Development* dev.183186. doi:10.1242/dev.183186

Kelly OG, Pinson KI, Skarnes WC. 2004. The Wnt co-receptors Lrp5 and Lrp6 are essential for gastrulation in mice. *Development* **131**:2803–2815. doi:10.1242/dev.01137

Kiyomitsu T, Cheeseman IM. 2013. XCortical dynein and asymmetric membrane elongation coordinately position the spindle in anaphase. *Cell* **154**:391. doi:10.1016/j.cell.2013.06.010

Knoblich JA, Jan LY, Jan YN. 1995. Asymmetric segregation of numb and prospero during cell division. *Nature* **377**:624–627. doi:10.1038/377624a0

Koltover I, Rädler JO, Safinya CR. 1999. Membrane mediated attraction and ordered aggregation of colloidal particles bound to giant phospholipid vesicles. *Phys Rev Lett* **82**:1991–1994. doi:10.1103/PhysRevLett.82.1991

Kornberg TB, Roy S. 2014. Cytonemes as specialized signaling filopodia. *Dev* **141**:729–736. doi:10.1242/dev.086223

Krause M, Dent EW, Bear JE, Loureiro JJ, Gertler FB. 2003. Ena/VASP Proteins: Regulators of the Actin Cytoskeleton and Cell Migration. *Annu Rev Cell Dev Biol* **19**:541–564. doi:10.1146/annurev.cellbio.19.050103.103356

Lerma J, Marques JM. 2013. Kainate receptors in health and disease. *Neuron* **80**:292–311. doi:10.1016/j.neuron.2013.09.045

Lian G, Dettenhofer M, Lu J, Downing M, Chenn A, Wong T, Sheen V. 2016. Filamin A- and formin 2-dependent endocytosis regulates proliferation via the canonical wnt pathway. *Dev* **143**:4509–4520. doi:10.1242/dev.139295

Liu SJ, Zukin RS. 2007. Ca2+-permeable AMPA receptors in synaptic plasticity and neuronal death. *Trends Neurosci* **30**:126–134. doi:10.1016/j.tins.2007.01.006

Lowndes M, Junyent S, Habib SJ. 2017. Constructing cellular niche properties by localized

presentation of Wnt proteins on synthetic surfaces. *Nat Protoc* **12**:1498–1512. doi:10.1038/nprot.2017.061

MacDonald BT, Semenov M V., Huang H, He X. 2011. Dissecting molecular differences between Wnt coreceptors LRP5 and LRP6. *PLoS One* **6**. doi:10.1371/journal.pone.0023537

Maddock JR, Shapiro L. 1993. Polar location of the chemoreceptor complex in the Escherichia coli cell. *Science (80-)* **259**:1717–1723. doi:10.1126/science.8456299

Martello G, Smith A. 2014. The nature of embryonic stem cells. *Annu Rev Cell Dev Biol* **30**:647–675. doi:10.1146/annurev-cellbio-100913-013116

Mizumoto K, Sawa H. 2007. Cortical β-Catenin and APC Regulate Asymmetric Nuclear β-Catenin Localization during Asymmetric Cell Division in C. elegans. *Dev Cell* **12**:287–299. doi:10.1016/j.devcel.2007.01.004

Morhenn VB, Waleh NS, Mansbridge JN, Unson D, Zolotorev A, Cline P, Toll L. 1994. Evidence for an NMDA receptor subunit in human keratinocytes and rat cardiocytes. *Eur J Pharmacol Mol Pharmacol* **268**:409–414. doi:10.1016/0922-4106(94)90066-3

Niciu MJ, Kelmendi B, Sanacora G. 2012. Overview of glutamatergic neurotransmission in the nervous system. *Pharmacol Biochem Behav* **100**:656–664. doi:10.1016/j.pbb.2011.08.008

Ortiz-Ramírez C, Michard E, Simon AA, Damineli DSC, Hernández-Coronado M, Becker JD, Feijó JA. 2017. GLUTAMATE RECEPTOR-LIKE channels are essential for chemotaxis and reproduction in mosses. *Nature* **549**:91–95. doi:10.1038/nature23478

Ouspenskaia T, Matos I, Mertz AF, Fiore VF, Fuchs E. 2016. WNT-SHH Antagonism Specifies and Expands Stem Cells prior to Niche Formation. *Cell* **164**:156–169. doi:10.1016/j.cell.2015.11.058

Peng CY, Manning L, Albertson R, Doe CQ. 2000. The tumour-suppresor genes lgl and dlg regulate basal protein targeting in Drosophila neuroblasts. *Nature* **408**:596–600. doi:10.1038/35046094

Raggioli A, Junghans D, Rudloff S, Kemler R. 2014. Beta-Catenin Is Vital for the Integrity of Mouse Embryonic Stem Cells. *PLoS One* **9**:e86691. doi:10.1371/journal.pone.0086691

Ran FA, Hsu PD, Wright J, Agarwala V, Scott DA, Zhang F. 2013. Genome engineering using the CRISPR-Cas9 system. *Nat Protoc* **8**:2281–2308. doi:10.1038/nprot.2013.143

Rangamani P, Lipshtat A, Azeloglu EU, Calizo RC, Hu M, Ghassemi S, Hone J, Scarlata S,

Neves SR, Iyengar R. 2013. XDecoding Information in Cell Shape. *Cell* **154**:1356. doi:10.1016/j.cell.2013.08.026

Schmick M, Bastiaens PIH. 2014. The interdependence of membrane shape and cellular signal processing. *Cell* **156**:1132–1138. doi:10.1016/j.cell.2014.02.007

Schober M, Schaefer M, Knoblich JA. 1999. Bazooka recruits inscuteable to orient asymmetric cell divisions in Drosophila neuroblasts. *Nature* **402**:548–551. doi:10.1038/990135

Skerry TM, Genever PG. 2001. Glutamate signalling in non-neuronal tissues. *Trends Pharmacol Sci* **22**:174–181. doi:10.1016/S0165-6147(00)01642-4

Sugioka K, Mizumoto K, Sawa H. 2011. Wnt regulates spindle asymmetry to generate asymmetric nuclear β-catenin in C. elegans. *Cell* **146**:942–954. doi:10.1016/j.cell.2011.07.043

Tamai K, Semenov M, Kato Y, Spokony R, Liu C, Katsuyama Y, Hess F, Saint-Jeannet JP, He X. 2000. LDL-receptor-related proteins in Wnt signal transduction. *Nature* **407**:530–535. doi:10.1038/35035117

Traynelis SF, Wollmuth LP, McBain CJ, Menniti FS, Vance KM, Ogden KK, Hansen KB, Yuan H, Myers SJ, Dingledine R. 2010. Glutamate Receptor Ion Channels: Structure, Regulation, and Function. *Pharmacol Rev* **62**:405–496. doi:10.1124/pr.109.002451

Walston T, Tuskey C, Edgar L, Hawkins N, Ellis G, Bowerman B, Wood W, Hardin J. 2004. Multiple Wnt signaling pathways converge to orient the mitotic spindle in early C. elegans embryos. *Dev Cell* **7**:831–841. doi:10.1016/j.devcel.2004.10.008

Wehrli M, Dougan ST, Caldwell K, O'Keefe L, Schwartz S, Valzel-Ohayon D, Schejter E, Tomlinson A, DiNardo S. 2000. Arrow encodes an LDL-receptor-related protein essential for Wingless signalling. *Nature* **407**:527–530. doi:10.1038/35035110

Yang G, Huang A, Zhu S, Xiong W. 2006. It is time to move: Role of lateral diffusion in AMPA receptor trafficking. *J Neurosci* **26**:9082–9083. doi:10.1523/JNEUROSCI.3018-06.2006

Yu C han, Wu HJ, Kaizuka Y, Vale RD, Groves JT. 2010. Altered actin centripetal retrograde flow in physically restricted immunological synapses. *PLoS One* **5**:1–9. doi:10.1371/journal.pone.0011878

Zhu Y, Tian Y, Du J, Hu Z, Yang L, Liu J, Gu L. 2012. Dvl2-dependent activation of Daam1 and RhoA regulates Wnt5a-induced breast cancer cell migration. *PLoS One* **7**.

doi:10.1371/journal.pone.0037823

FIGURE LEGENDS

Figure 1. Wnt3a responsiveness and formation of dynamic cytonemes in Wnt/β-catenin pathway KO ESCs

A. Simplified schematic representation of the Wnt/β-catenin pathway. Wnt3a binding to the receptor Frizzled and the co-receptors Lrp5 and Lrp6 induces the inhibition of the β-catenin destruction complex (Axin2, Gsk3, Ck1, APC) through Dvl. β-catenin is stabilized and translocated to the nucleus, where it binds Tcf/Lef to initiate the transcription of Wnt3a target genes.

B. (*Top-left*) Schematic representation of the 7xTCF-eGFP Wnt/β-catenin reporter. (*Top-right* and *Bottom*) Representative dot-plots depicting the levels of eGFP expression in WT or Wnt pathway KO ESCs carrying the 7xTCF-eGFP reporter and treated with CNTRL solution or 200 ng/mL soluble Wnt3a for 24h. Y axis is SSC. Values in plots are percentage of GFP+ cells.

C. Percentage of 7xTCF-eGFP$^+$ cells measured by FACS, as described in **B**. n = 6 for WT, n = 3 for KO ESCs. Bars and numbers are mean, error bars indicate SEM. Stars indicate statistical significance calculated by two-way ANOVA with Dunnett's multiple comparison test: ****$p < 0.0001$.

D. Relative *Axin2* expression in WT or Wnt pathway KO ESCs treated with CNTRL media or 200 ng/mL soluble Wnt3a for 24h, measured by qPCR. n = 3. Bars and numbers are geometric mean, error bars indicate geometric SD. Stars indicate statistical significance calculated by two-way ANOVA with Dunnett's multiple comparison test: ****$p < 0.0001$.

E. Representative images of the cytonemes in WT, Lrp5KO (#1), Lrp6KO (#1), Lrp5/6dKO (#1) and βKO ESCs. Cells were stained with Cell Mask Deep Red and imaged for 10 sec every 10 min on a spinning disk confocal, with a 40x/0.95 air objective (incubation at 37°C, 5%CO_2). Insets (*below*) are magnifications of black dashed boxes, contrast-enhanced for clarity. Yellow arrowheads indicate thin protrusions. Time is in seconds. Scale-bars are 10 µm.

Numeric data used in the figure can be found in the Source Data file.

Figure 1 – Figure Supplement 1. Genotype of Wnt co-receptor KO ESCs

A – C. Schematic representations of the genotype of Lrp5KO (#2) (**A**), Lrp6KO (#2) (**B**) and Lrp5/6dKO (#2) (**C**). "CRISPR" sequence indicates the gRNA sequence used for the gene editing, red NGG sequences indicate adjacent PAM (or CCN for reverse complement). "WT"

sequences indicate wildtype gene and “KO” sequences indicate modified gene sequences (homozygous). Dashes indicate deleted base-pairs.

Figure 1 – Figure Supplement 2. Representative images of cytonemes in Wnt co-receptor KO ESCs

Representative images of the cytonemes in Lrp5KO (#2), Lrp6KO (#2), Lrp5/6dKO (#2) ESCs. Cells were stained and imaged as described in **Figure 1E**. Insets (*below*) are magnifications of black dashed boxes, contrast-enhanced for clarity. Yellow arrowheads indicate thin protrusions. Time is in seconds. Scale-bars are 10 µm.

Figure 2. Lrp5 controls the generation of cytonemes by ESCs

A – D. Percentage of WT, Lrp5KO (clone #1 and #2) (**A**), Lrp6KO (#1 and #2) (**B**), Lrp5/6dKO (#1 and #2) (**C**) and βKO ESCs (**D**) with cytonemes at 0 to 4h after seeding. Line and dots are mean, error bars are SEM. N ≥ 33 cells, n ≥ 3 experiments. Stars and symbols in box (right of each plot) indicate statistical significance to WT ESCs, calculated by two-way ANOVA with Dunnett’s multiple comparison test (for **A** – **C**) or multiple unpaired t-tests (for **D**): ns (non-significant, *p>0.05*), **p<0.05*, ***p<0.01*, ****p<0.001*, *****p<0.0001*. The same WT ESCs data is presented in **A** – **D** for comparison.

E. Cell movement, presented as mean squared displacement per minute (MSD) for WT ESCs co-cultured with Wnt3a- or iWnt3a-beads, or Wnt/β-catenin pathway KO ESCs co-cultured with Wnt3a-beads. n ≥ 36 cells, pooled from ≥ 3 independent experiments, were tracked for 3h after attachment. Box represents median and quartiles, error bars are 10-90 percentile, dots are data outside 10-90 range. ns indicates non-significant (*p>0.05*) differences calculated by one-way ANOVA with Dunnett’s multiple comparison test.

Numeric data used in the figure can be found in the Source Data file.

Figure 3. Lrp6 and β-catenin are required for Wnt3a-bead accumulation

A – E. Percentage of WT, Lrp5KO (#1 and #2) (**B**), Lrp6KO (#1 and #2) (**C**), Lrp5/6dKO (#1 and #2) (**C**) and βKO (**E**) ESCs contacting Wnt3a-beads or iWnt3a beads (indicated in brackets) at 0 to 12h after seeding. Line and dots are mean, error bars are SEM. N ≥ 36 cells, n ≥ 3 experiments. The same WT ESCs + Wnt3a-beads data is presented in **A** – **E** for comparison.

F. Statistical analysis of **A** – **E**, calculated for all conditions against WT ESCs + Wnt3a-beads. Stars and symbols indicate statistical significance calculated by two-way ANOVA with Dunnett’s multiple comparison tests: ns (non-significant, *p>0.05*), **p<0.05*, ***p<0.01*, ****p<0.001*, *****p<0.0001*.

Numeric data used in the figure can be found in the Source Data file.

Figure 4. Wnt co-receptors and β-catenin orchestrate the interaction between ESCs and Wnt3a-beads at the membrane

A. Representative brightfield frames of time-course live imaging sequences displaying an ESC contacting a Wnt3a-bead without recruitment (*left*), contact with recruitment (*middle*) and a Wnt3a-bead recruitment with subsequent dropping (*right*). Scale-bars are 20 µm. Wnt3a-beads are highlighted by white dashed circles.

B. Representative brightfield image of an ESC contacting a Wnt3a-bead (*right*). Schematic representation of the cell "periphery" (1-0.7 proportion of radius, brown), 0.7-0.3 proportion of radius (orange) or "centre" of the cell (0.3-0 proportion of radius, yellow), and of the radius used to calculate the bead position (white line) (*right*). Scale-bar is 20 µm. Wnt3a-bead is highlighted by white dashed circles.

C – G. Wnt3a-bead position in the cell, measured every minute for 3h (180 min) after initial cytoneme-mediated recruitment, and presented as ratio to cell radius. Lines are mean of n ≥ 38 cells/condition, pooled approximately evenly from ≥ 3 independent experiments. Single cell tracks are presented in **Figure 4 - Figure Supplement 1**. Stars or symbols are statistical significance, calculated from the average Wnt3a-bead position per cell in three representative time windows (0 to 30 min, 31 to 120 min and 121 to 180 min) against the position of Wnt3a-beads in WT ESCs, by two-way ANOVA with Dunnett's (**D - F**) or Šídák's (**C and G**) multiple comparison test: ns (non-significant, $p>0.05$), *$p<0.05$, **$p<0.01$, ****$p<0.0001$. The same WT ESCs + Wnt3a-beads data is presented in **C** – **G** for comparison.

H. Representative brightfield frames of a time-course live imaging, showing an ESC contacting a Wnt3a-bead (highlighted with white dashed circle). Yellow track indicates Wnt3a-bead movement on the cell over time. Time is in minutes. Scale-bar is 20 µm.

I. Wnt3a-bead movement on the cell, presented as mean squared displacement per minute (MSD). Bead movement was measured every minute for 3h (180 min) after cytoneme-mediated recruitment in WT ESCs contacting Wnt3a- or iWnt3a-beads, and in Wnt pathway KO ESCs contacting Wnt3a-beads. Box indicates median and quartiles, error bars indicate 10-90 percentile, dots are data outside 10-90 percentile range. n ≥ 38 cells pooled approximately evenly from ≥ 3 independent experiments. Stars indicate statistical significance against WT ESCs + Wnt3a-beads, calculated by one-way ANOVA with Dunnett's multiple comparison test: ns (non-significant, $p>0.05$), *$p<0.05$, **$p<0.01$, ***$p<0.001$.

J. Percentage of cells that drop a Wnt3a-bead or iWnt3a-bead within 3h of initial recruitment with a cytoneme (grey) or retain it for longer than 3h (blue). n ≥ 43 cells/condition. Stars indicate statistical significance calculated by multiple Fisher's exact tests: ns (non-significant, *p>0.05*), **p<0.05*, ****p<0.0001*.

Numeric data used in the figure can be found in the Source Data file.

Figure 4 – Figure Supplement 1. Details of Wnt3a-bead position in WT or Wnt/β-catenin pathway KO ESCs membrane

A – I. Detailed quantification of the Wnt3a-bead position on the membrane of WT or Wnt/β-catenin KO ESCs after initial cytoneme-mediated recruitment, including single-cell tracked positions (grey lines) and mean position per condition (coloured line).

Numeric data used in the figure can be found in the Source Data file.

Figure 5. iGluR inhibition or KO does not affect cytoneme-independent Wnt3a responsiveness

A. Relative expression of *Axin2* mRNA in a monolayer of WT, GriA3/4dKO or GriK1/3dKO ESCs treated with control media (CNTRL), solubilized Wnt3a (200 ng/mL) or a high density of Wnt3a-beads for 24h. Bars are mean of n = 3, error bars are SEM. Stars indicate statistical significance, calculated by two-way ANOVA with Tukey's multiple comparison test: ***p<0.01*, ****p<0.001*, *****p<0.0001*.

B. Percentage of 7xTCF-eGFP^{+} cells in control- or CNQX-treated cells upon addition of control solution (CNTRL), solubilized Wnt3a (200 ng/mL), Wnt3a-beads or iWnt3a-beads at coating concentrations. Bars are mean of n = 3, error bars are SEM. Stars indicate statistical significance calculated by one-way ANOVA with Šídák's multiple comparison test: *****p<0.0001*.

C. Representative brightfield image of a monolayer of cells treated with Wnt3a-beads. Scale-bar is 50 µm.

Numeric data used in the figure can be found in the Source Data file.

Figure 5 – Figure Supplement 1. Genotype of GriA3/4dKO and GriK1/3dKO ESCs.

A – D. Schematic representations of the genotype of GriA3/4dKO (clone #1 and #2) (**A and B**) and GriK1/3dKO (clone #1 and #2) ESCs (**C and D**). "CRISPR" sequence indicates the gRNA sequence used for the gene editing, red NGG sequences indicate adjacent PAM. "WT" sequences indicate wildtype gene and "KO" sequences indicate modified gene

sequences. For GriA3/4dKO (#2), two mutant sequences were detected at equal rates. Dashes indicate deleted base-pairs. Asterisk (*) indicates insertion.

Figure 6. iGluRs control Wnt3a-bead recruitment without affecting the generation and characteristics of the cytonemes.

A – B. Average number of cytonemes/cell (**A**) and maximum cytoneme length/cell (**B**) in WT, GriA3/4dKO, GriK1/3dKO and CNQX-treated ESCs. Boxes are median and quartiles, error-bars are 10-90 percentiles, dots are data outside range. n ≥ 25 cells/condition (**A** and **B**). "ns" are non-significant differences calculated against WT ESCs by one-way ANOVA with Dunnett's multiple comparison tests.

C – E. Percentage of WT, GriK1/3dKO (clone #1 and #2) (**C**), GriA3/4dKO (#1 and #2) (**D**) and CNQX-treated ESCs (**E**) with cytonemes at 0 to 4h after seeding. Line and dots are mean, error bars are SEM. N ≥ 38 cells, n ≥ 3 experiments. WT ESC data from **Fig. 2A** – **D** presented for comparison.

F. Statistical analysis of **C** – **E**. Stars and symbols in box indicate statistical significance of each condition to WT ESCs, calculated by two-way ANOVA with Dunnett's multiple comparison test (for **C** and **D**) or multiple unpaired t-tests (for **E**): ns (non-significant, *p>0.05*), ***p<0.01*, ****p<0.001*, *****p<0.0001*.

G – I. Percentage of WT, GriK1/3dKO (#1 and #2) (**G**), GriA3/4dKO (#1 and #2) (**H**) and CNQX-treated ESCs (**I**) contacting Wnt3a-beads at 0 to 12h after seeding. Line and dots are mean, error bars are SEM. N ≥ 36 cells, n ≥ 3 experiments. WT ESCs + Wnt3a-beads data from **Fig. 3A** – **E** presented for comparison.

J. Statistical analysis of **G** – **I**. Stars and symbols indicate statistical significance of each condition to WT ESCs, calculated by two-way ANOVA with Dunnett's multiple comparison tests: ns (non-significant, *p>0.05*), **p<0.05*, ***p<0.01*, ****p<0.001*, *****p<0.0001*.

K. Cell movement, presented as mean squared displacement per minute (MSD) for WT, GriK1/3dKO, GriA3/4dKO and CNQX-treated ESCs. n ≥ 44 cells, pooled from ≥ 3 independent experiments, were tracked for 3h after attachment. Box represents median and quartiles, error bars are 10-90 percentile, dots are data outside 10-90 range. Stars indicate statistical differences calculated by one-way ANOVA with Dunnett's multiple comparison test: **p<0.05*

Numeric data used in the figure can be found in the Source Data file.

Figure 6 – Figure Supplement 1. Representative images of cytonemes in GriK1/3dKO and GriA3/4dKO ESCs

Representative images of the cytonemes in GriK1/3dKO (clone #1 and #2) and GriA3/4dKO (clone #1 and #2) ESCs. Cells were stained and imaged as described in **Figure 1E**. Insets (*below*) are magnifications of black dashed boxes, contrast-enhanced for clarity. Yellow arrowheads indicate thin protrusions. Time is in seconds. Scale-bars are 10 µm.

Figure 7. GriK1/3dKO, GriA3/4dKO or CNQX-treated cells retain the beads further from the cell centre

A – C. Wnt3a-bead position in the cell surface, measured every minute for 3h (180 min) after initial cytoneme-mediated recruitment, and presented as proportion of cell radius. Lines are mean of n ≥ 45 cells/condition, pooled approximately evenly from ≥ 3 independent experiments. Single cell tracks are presented in **Figure 7 - Figure Supplement 1**. Stars or symbols are statistical significance, calculated from the average Wnt3a-bead position per cell in three representative time windows (0 to 30 min, 31 to 120 min and 121 to 180 min) against the position of Wnt3a-beads in WT ESCs, by two-way ANOVA with Dunnett's multiple comparison test: ns (non-significant, $p>0.05$), *$p<0.05$, **$p<0.01$, ***$p<0.001$, ****$p<0.0001$. WT ESCs + Wnt3a-beads data from **Fig. 4C** – **G** presented for comparison.

D. Wnt3a-bead movement on the cell, presented as mean squared displacement per minute (MSD). Bead movement was measured every minute for 3h (180 min) after cytoneme-mediated recruitment in WT GriK1/3dKO, GriA3/4dKO and CNQX-treated ESCs contacting Wnt3a-beads. Box indicates median and quartiles, error bars indicate 10-90 percentile, dots are data outside 10-90 percentile range. n ≥ 45 cells pooled approximately evenly from ≥ 3 independent experiments. Stars indicate statistical significance against WT ESCs + Wnt3a-beads, calculated by one-way ANOVA with Dunnett's multiple comparison test: ns (non-significant, $p>0.05$), *$p<0.05$, ***$p<0.001$.

E. Percentage of cells that drop a Wnt3a-bead within 3h of initial recruitment with a cytoneme (grey) or retain it for longer than 3h (blue). n ≥ 37 cells/condition. ns is non-significant differences calculated by multiple Fisher's exact tests.

Numeric data used in the figure can be found in the Source Data file.

Figure 7 – Figure Supplement 1. Details of Wnt3a-bead position in WT, GriK1/3dKO, GriA3/4dKO and CNQX-treated ESCs membrane

A – E. Detailed quantification of the Wnt3a-bead position on the membrane of WT, GriK1/3dKO, GrA3/4dKO and CNQX-treated ESCs after initial cytoneme-mediated recruitment, including single-cell tracked positions (grey lines) and mean position per condition (coloured line).

Numeric data used in the figure can be found in the Source Data file.

Figure 8. Components of the Wnt/β-catenin pathway regulate the orientation of the mitotic spindle of ESCs

A. Representative brightfield frames of a time course live-cell imaging, showing an ESC contacting a Wnt3a-bead and undergoing Wnt3a-oriented division. Wnt3a-bead is black sphere. Dashed black box indicates the "Anaphase" timepoint used for spindle orientation analysis. Scale-bar is 10 µm.

B. (*Left*) Representative image of the method used for spindle angle measurement relative to Wnt3a-bead position. Asterisks indicate cell poles used as reference for the measurement. Orthogonal white lines depict major and minor axis, yellow line points to Wnt3a-bead and shows the angle measured (α). Wnt3a-bead is highlighted with yellow dashed circle. (*Right*) Representative images of different ESCs dividing with Wnt3a-beads at angles between 0 and 90° (indicated in the figure). Scale-bars are 10 µm.

C – K. Rose plots depicting the distribution of spindle angles in WT ESCs dividing with Wnt3a-beads (**C**), WT ESCs dividing with iWnt3a-beads (**D**) or Lrp5KO ESCs (**E** and **F**), Lrp6KO ESCs (**G** and **H**), Lrp5/6dKO ESCs (**I** and **J**) and βKO ESCs (**K**) dividing with Wnt3a-beads. n (number of cells analysed) is depicted in the figure for each condition.

L. Statistical comparison of the distribution of spindle angles in all conditions to the one observed in WT ESCs + Wnt3a beads. Stars indicate statistical significance calculated by multiple Kolmogorov-Smirnov tests: ***p<0.01*, ****p<0.001*, *****p<0.0001.*

Numeric data used in the figure can be found in the Source Data file.

Figure 9. β-catenin and Lrp6 are required for Wnt3a-mediated ACD

A. Representative images of ESC doublets after dividing in contact with a Wnt3a-bead, labelled with antibodies against Nanog (cyan), Rex1 (magenta) and Sox2 (greyscale), or with 4′,6-diamidino-2-phenylindole (DAPI, yellow). Images are maximum intensity projections of a selected Z-stack. DIC is differential interference contrast. Panels display doublets with higher marker expression in the Wnt3a-bead contacting cell (*top*, "Proximal"), with equal levels of expression between both cells (*middle*, "Distributed") or with higher marker expression in the cell not contacting the Wnt3a-bead (*bottom*, "Distal"). The Wnt3a-beads are highlighted by yellow dashed circles. Scale-bars are 20 µm.

B – C. Percentage of doublets of WT or Wnt/β-catenin KO ESCs contacting Wnt3a-beads or iWnt3a-beads in the "Proximal", "Distributed" or "Distal" categories for Nanog (**B**), Rex1 (**C**) or Sox2 (**D**). n ≥ 3 experiments, with N ≥ 18 doublets/n (Nanog, Rex1) or N ≥ 28 doublets/n

(Sox2). For **D**. only clone #2 of Lrp5KO, Lrp6KO and Lrp5/6dKO ESCs were analysed. Box indicates median and quartiles, error bars indicate 10-90 percentile. Dots are data outside range. Stars and symbols indicate statistical significance for each condition against WT ESCs + Wnt3a beads, calculated by two-way ANOVA with Dunnett's multiple comparison test: ns (non-significant, $p>0.05$), *$p<0.05$, **$p<0.01$, ***$p<0.001$, ****$p<0.0001$.

Numeric data used in the figure can be found in the Source Data file.

Figure 10. Lrp6 overexpression in Lrp5/6dKO ESCs rescues ACD

A. Schematic of the experimental pipeline. Lrp5/6dKO (#2) ESCs were transfected with pEGFP-Lrp6 plasmids and sorted by FACS to Lrp6-expressing (GFP^+) and Lrp6 non-expressing (GFP^-) populations before experimentation.

B. Representative dot-plot of GFP expression levels in Lrp5/6dKO control (non-transfected) ESCs or Lrp5/6dKO ESCs transfected with pEGFP-Lrp6. GFP intensity was detected using a FITC filter. Y axis is PE. GFP^- (blue) and GFP^+ (magenta) cells were sorted only in the transfected condition.

C. Rose plots depicting the distribution of spindle angle orientations in GFP^+ or GFP^- ESCs dividing in contact with a Wnt3a-bead. Stars and symbols in boxes (*right*) indicate statistical significance calculated by multiple Kolmogorov-Smirnov tests against GFP^+ ESCs (*top*) or WT ESCs dividing with a Wnt3a-bead (*bottom*): ns (non-significant, $p>0.05$), ***$p<0.001$, ****$p<0.0001$. n (number of cells) is depicted in the figure.

D. Representative images of GFP^+ and GFP^- ESCs after dividing with a Wnt3a-bead, stained with antibodies against Sox2 (cyan) and Nanog (magenta), or with DAPI (yellow). Wnt3a-beads are highlighted by yellow dashed circle. Scale-bars are 20 µm.

E and F. Percentage of doublets in the "Proximal", "Distributed" or "Distal" categories (described in **Fig. 9A**) in GFP^+ and GFP^- ESCs stained for Sox2 (**E**) and Nanog (**F**). Mean of n = 3 independent experiments, N ≥ 29 doublets analysed per n, error bars are SEM. Stars indicate statistical significance calculated by two-way ANOVA with Šídák's multiple comparison tests: *$p<0.05$, **$p<0.01$, ***$p<0.001$.

Numeric data used in the figure can be found in the Source Data file.

Figure 11. AMPA-type iGluR receptors are important for Wnt3a-oriented ACD.

A and B. Rose plots depicting the distribution of spindle orientations in GriK1/3dKO, GriA3/4dKO or CNQX-treated ESCs (**A**) or DMSO- or NBQX-treated ESCs (**B**) dividing with a Wnt3a-bead. n (number of cells analysed) is stated in the figures. Stars in boxes indicate

statistical significance calculated by multiple Kolmogorov-Smirnov test against WT ESCs + Wnt3a-beads (in **A**) or DMSO-treated ESCs + Wnt3a-beads (in **B**): ***p<0.01*, ****p<0.0001*.

C – E. Percentage of doublets in the "Proximal", "Distributed" or "Distal" categories (described in **Fig. 9A**) for WT, GriK1/3dKO, GriA3/4dKO or CNQX-treated ESCs that have divided with Wnt3a-beads. Quantification for Nanog (**C**), Rex1 (**D**) or Sox2 (**E**). n ≥ 3 experiments, with N ≥ 18 doublets/n (Nanog, Rex1) or N ≥ 30 doublets/n (Sox2). Box indicates median and quartiles, error bars indicate 10-90 percentile. Dots are data outside range. Stars and symbols indicate statistical significance calculated by two-way ANOVA with Dunnett's multiple comparison test: ns (non-significant, *p>0.05*), **p<0.05*, ***p<0.01*, ****p<0.001*, *****p<0.0001*. WT ESC data from **Fig. 9B** – **D** presented for comparison.

F – H. Percentage of doublets in the "Proximal", "Distributed" or "Distal" categories (described in **Fig. 9A**) for DMSO- or NBQX-treated ESCs that have divided with a Wnt3a-bead. Quantification for Nanog (**F**), Rex1 (**G**) or Sox2 (**H**). n = 4 experiments, with N = 30 doublets/n. Box indicates median and quartiles, error bars indicate 10-90 percentile. Stars indicate statistical significance calculated by two-way ANOVA with Šídák's multiple comparison tests: **p<0.05*, ***p<0.01, ****p<0.001.*

Numeric data used in the figure can be found in the Source Data file.

CAPTIONS FOR MOVIES

Movie 1. WT ESC cytonemes. High-quality images of the dynamic cytonemes of WT ESCs. Cells were stained with Cell Mask Deep Red and imaged in a spinning disk confocal microscope every 10 sec, for 10 min. Images are presented as inverted grayscale. Yellow boxes are magnifications, contrast-enhanced for clarity. Time is minutes and seconds. Scale bar, 10 µm.

Movie 2. Lrp5KO ESC cytonemes. High-quality images of the dynamic cytonemes of Lrp5KO ESCs (clone #1 and #2). Cells were stained and imaged as described for **Movie 1**. Images are presented as inverted grayscale. Yellow boxes are magnifications, contrast-enhanced for clarity. Time is minutes and seconds. Scale bar, 10 µm.

Movie 3. Lrp6KO ESC cytonemes. High-quality images of the dynamic cytonemes of Lrp6KO ESCs (clone #1 and #2). Cells were stained and imaged as described for **Movie 1**. Images are presented as inverted grayscale. Yellow boxes are magnifications, contrast-enhanced for clarity. Time is minutes and seconds. Scale bar, 10 µm.

Movie 4. Lrp5/6dKO ESC cytonemes. High-quality images of the dynamic cytonemes of Lrp5/6dKO ESCs (clone #1 and #2). Cells were stained and imaged as described for **Movie**

1. Images are presented as inverted grayscale. Yellow boxes are magnifications, contrast-enhanced for clarity. Time is minutes and seconds. Scale bar, 10 µm.

Movie 5. βKO ESC cytonemes. High-quality images of the dynamic cytonemes of βKO ESCs. Cells were stained and imaged as described for **Movie 1**. Images are presented as inverted grayscale. Yellow boxes are magnifications, contrast-enhanced for clarity. Time is minutes and seconds. Scale bar, 10 µm

Movie 6. Tracking of ESCs and Wnt3a beads. Time-course live-cell brightfield images of a WT or Lrp6KO ESC interacting with a Wnt3a-bead. Cell centre and Wnt3a-bead were tracked for 180 min, and the tracks are displayed. Scale bars, 20 µm.

Movie 7. GriA3/4dKO ESC cytonemes. High-quality images of the dynamic cytonemes of GriA3/4dKO ESCs (clone #1 and #2). Cells were stained and imaged as described for **Movie 1**. Images are presented as inverted grayscale. Yellow boxes are magnifications, contrast-enhanced for clarity. Time is minutes and seconds. Scale bar, 10 µm.

Movie 8. GriK1/3dKO ESC cytonemes. High-quality images of the dynamic cytonemes of GriK1/3dKO ESCs (clone #1 and #2). Cells were stained and imaged as described for **Movie 1**. Images are presented as inverted grayscale. Yellow boxes are magnifications, contrast-enhanced for clarity. Time is minutes and seconds. Scale bar, 10 µm.

Movie 9. Spindle orientation in dividing ESCs with Wnt3a-beads. Time-course live-cell brightfield images of a WT ESC dividing with Wnt3a-beads at ~90°, ~45° or ~0°. Spindle orientation angle was always measured at anaphase. White lines in stills indicate minor and major axis of the cell. Yellow line indicates the position of the Wnt3a-bead relative to the minor axis. Scale bars, 20 µm.

Figure 1

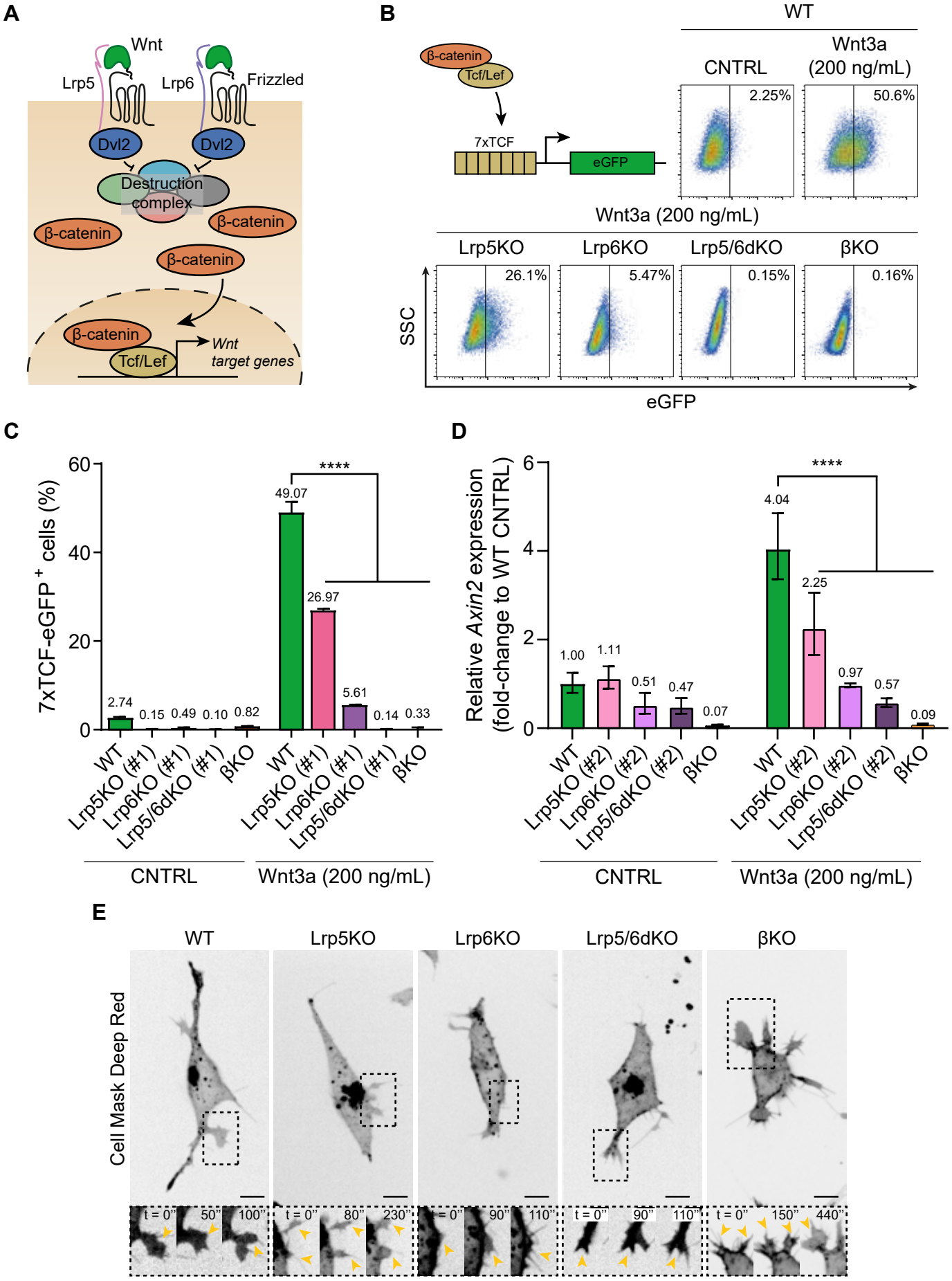
A
Wnt
Lrp5
Lrp6
Frizzled
Dvl2
Dvl2
Destruction complex
β-catenin
β-catenin
β-catenin
β-catenin
Tcf/Lef
Wnt target genes
B
β-catenin
Tcf/Lef
7xTCF
eGFP
WT
CNTRL
Wnt3a (200 ng/mL)
2.25%
50.6%
Wnt3a (200 ng/mL)
Lrp5KO
Lrp6KO
Lrp5/6dKO
βKO
26.1%
5.47%
0.15%
0.16%
SSC
eGFP
C
7xTCF-eGFP+ cells (%)
60
40
20
0
****
49.07
26.97
5.61
0.14
0.33
2.74
0.15
0.49
0.10
0.82
WT
Lrp5KO (#1)
Lrp6KO (#1)
Lrp5/6dKO (#1)
βKO
CNTRL
Wnt3a (200 ng/mL)
D
Relative Axin2 expression (fold-change to WT CNTRL)
6
4
2
0
****
4.04
2.25
0.97
0.57
0.09
1.00
1.11
0.51
0.47
0.07
WT
Lrp5KO (#2)
Lrp6KO (#2)
Lrp5/6dKO (#2)
βKO
CNTRL
Wnt3a (200 ng/mL)
E
WT
Lrp5KO
Lrp6KO
Lrp5/6dKO
βKO
Cell Mask Deep Red
t = 0"
50"
100"
t = 0"
80"
230"
t = 0"
90"
110"
t = 0"
90"
110"
t = 0"
150"
440"

Figure 1 - Supplement 1

A Lrp5KO (#2)

Lrp5 (Chromosome 19, NC_000085.6) 10bp deletion

PAM
CCGGGATGTGCGGCTAGTGG CRISPR

5' CTGTTGTTTGCCAACCG**CCGGGATGTGCGGCTAGTGG**ATGCCGGC 3' WT
5' CTGTTGTTTGCCAACCG**CCGG**−−−−−−−−−−**TAGTGG**ATGCCGGC 3' KO
DNA

B Lrp6KO (#2)

Lrp6 (Chromosome 6, NC_000072.6) 19bp deletion

PAM
ACAGAGATTTACTGGCCAAA CRISPR

5' TATAATAAAC**ACAGAGATTTACTGGCCAAA**CGGACTGACTCTGGACT 3' WT
5' TATAATAAAC**ACAGAGATTT**−−−−−−−−−−−−−−−−−−−TCTGGACT 3' KO
DNA

C Lrp5/6dKO (#2)

Lrp5 (Chromosome 19, NC_000085.6) 2bp deletion

PAM
CCGGGATGTGCGGCTAGTGG CRISPR

5' CTGTTGTTTGCCAACCG**CCGGGATGTGCGGCTAGTGG**ATGCCGGC 3' WT
5' CTGTTGTTTGCCAACCG**C**−−**GGATGTGCGGCTAGTGG**ATGCCGGC 3' KO
DNA

Lrp6 (Chromosome 6, NC_000072.6) 10bp deletion

PAM
GTGCCAAAGATAGAACGTGC CRISPR

5' TGGGGAGAA**GTGCCAAAGATAGAACGTGC**TGGGATGGATGGCTCA 3' WT
5' TGGGGAGAA**GTGCCAA**−−−−−−−−−−**TGC**TGGGATGGATGGCTCA 3' KO
DNA

Figure 1 - Supplement 2

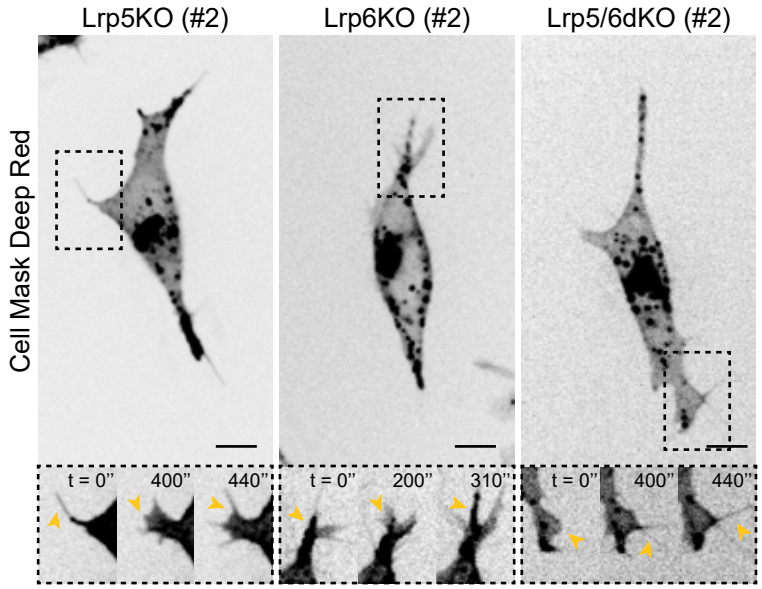

Figure 2

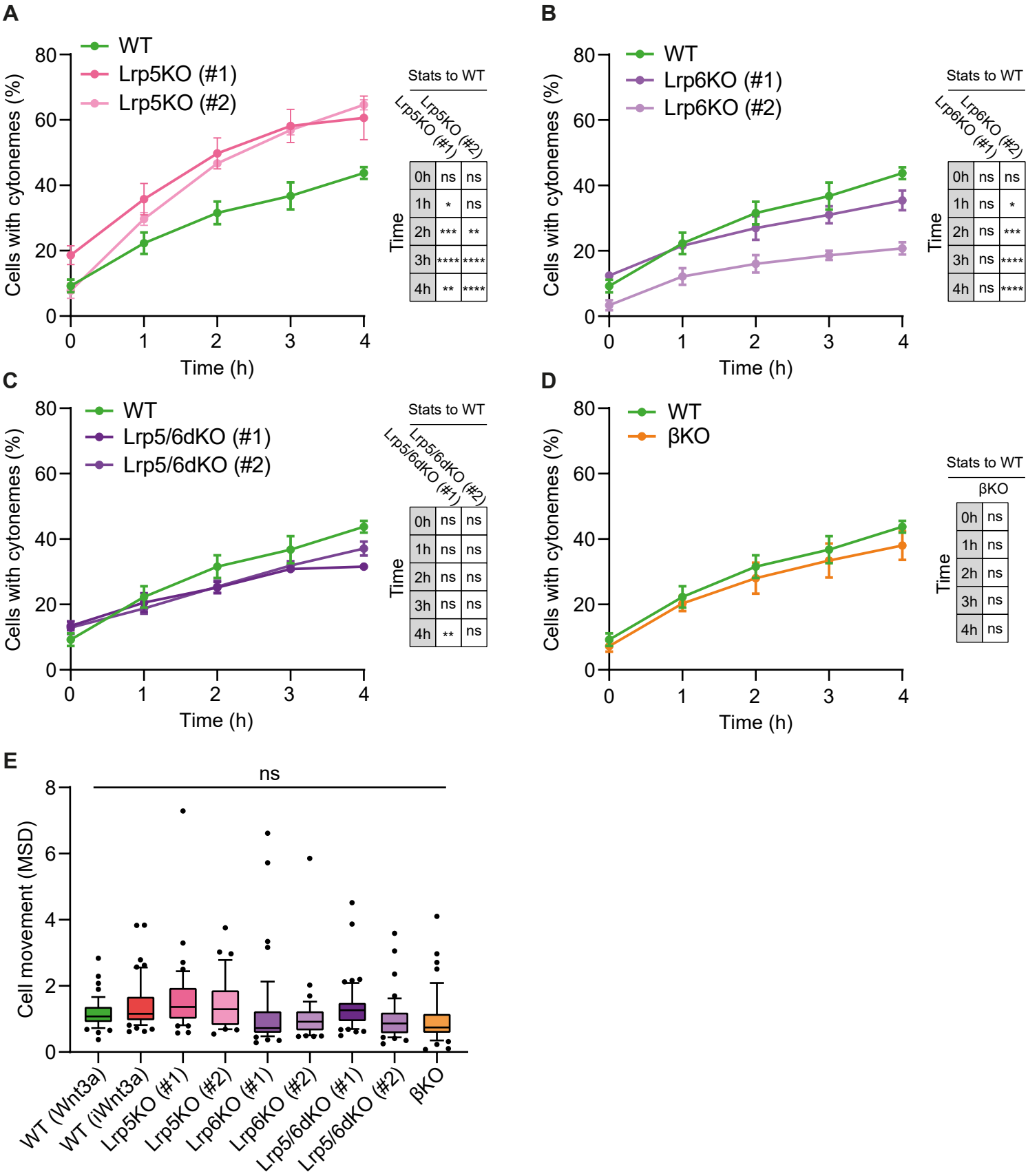
A
WT
Lrp5KO (#1)
Lrp5KO (#2)
Cells with cytonemes (%)
Time (h)
Stats to WT
Time
0h ns ns
1h * ns
2h *** **
3h **** ****
4h ** ****
B
WT
Lrp6KO (#1)
Lrp6KO (#2)
Cells with cytonemes (%)
Time (h)
Stats to WT
Time
0h ns ns
1h ns *
2h ns ***
3h ns ****
4h ns ****
C
WT
Lrp5/6dKO (#1)
Lrp5/6dKO (#2)
Cells with cytonemes (%)
Time (h)
Stats to WT
Time
0h ns ns
1h ns ns
2h ns ns
3h ns ns
4h ** ns
D
WT
βKO
Cells with cytonemes (%)
Time (h)
Stats to WT
Time
0h ns
1h ns
2h ns
3h ns
4h ns
E
ns
Cell movement (MSD)
WT (Wnt3a)
WT (iWnt3a)
Lrp5KO (#1)
Lrp5KO (#2)
Lrp6KO (#1)
Lrp6KO (#2)
Lrp5/6dKO (#1)
Lrp5/6dKO (#2)
βKO

Figure 3

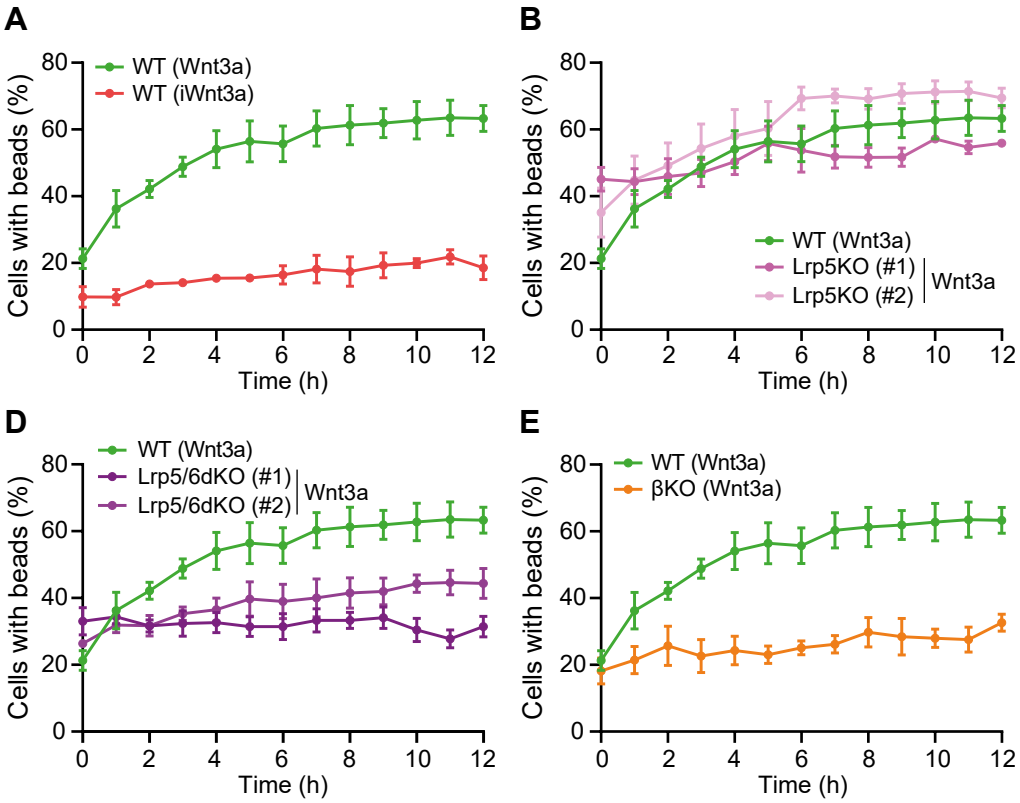

F

Time	Stats to WT (Wnt3a)	WT (iWnt3a)	Lrp5KO (#1)	Lrp5KO (#2)	Lrp6KO (#1)	Lrp6KO (#2)	Lrp5/6dKO (#1)	Lrp5/6dKO (#2)	βKO
0h	ns	***	ns	ns	ns	ns	ns	ns	ns
1h	***	ns	ns	ns	ns	ns	ns	ns	ns
2h	****	ns	ns	ns	ns	ns	ns	*	
3h	****	ns	ns	**	*	*	ns	***	
4h	****	ns	ns	***	**	**	*	****	
5h	****	ns	ns	***	**	***	*	****	
6h	****	ns	ns	***	*	***	*	****	
7h	****	ns	ns	****	**	***	**	****	
8h	****	ns	ns	****	**	****	**	****	
9h	****	ns	ns	****	*	****	**	****	
10h	****	ns	ns	****	**	****	*	****	
11h	****	ns	ns	***	***	****	*	****	
12h	****	ns	ns	****	***	****	*	****	

Figure 4

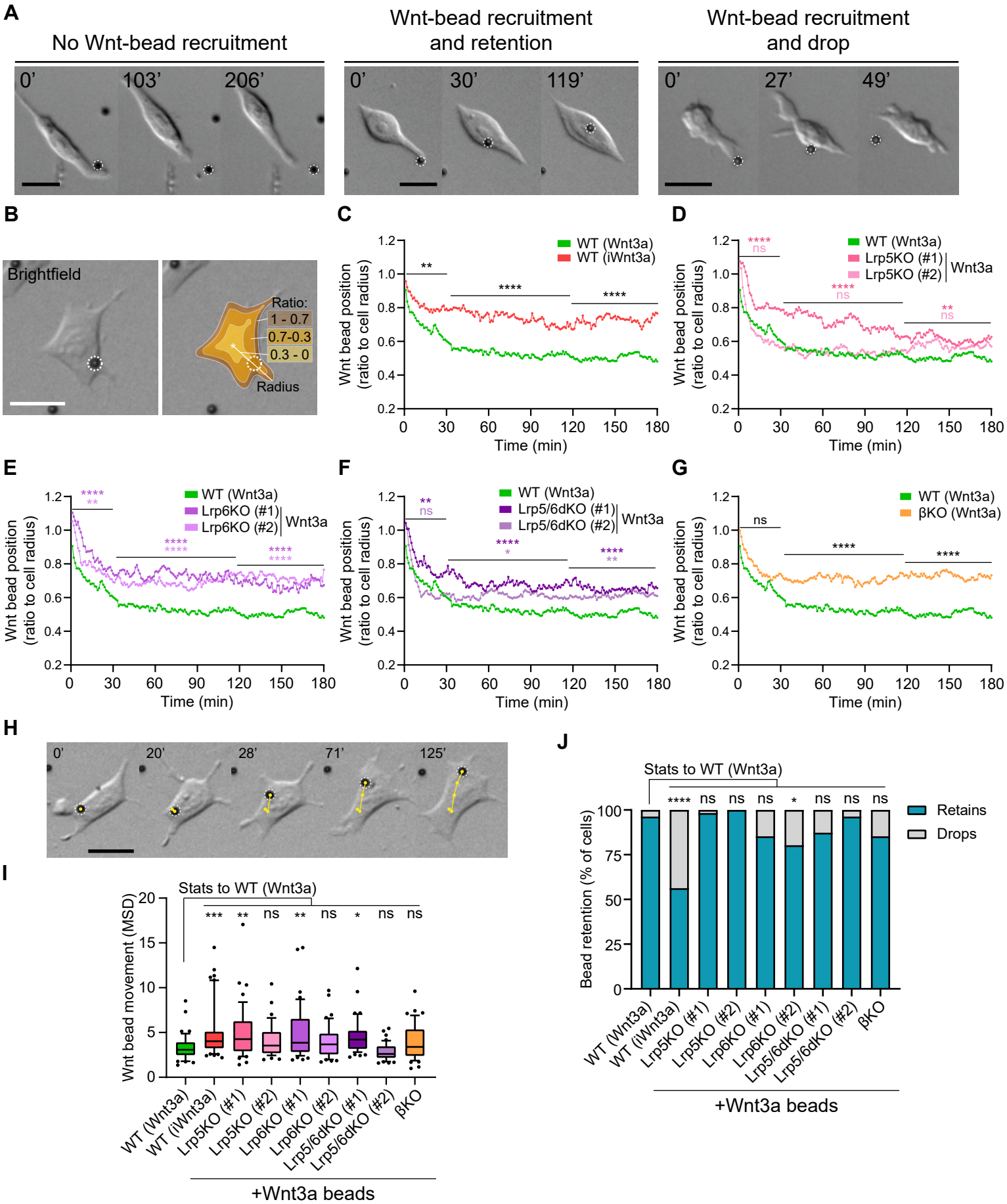
A
No Wnt-bead recruitment
Wnt-bead recruitment and retention
Wnt-bead recruitment and drop
0'
103'
206'
30'
119'
27'
49'
B
Brightfield
Ratio:
1 - 0.7
0.7-0.3
0.3 - 0
Radius
C
WT (Wnt3a)
WT (iWnt3a)
Wnt bead position (ratio to cell radius)
Time (min)
D
WT (Wnt3a)
Lrp5KO (#1)
Lrp5KO (#2)
Wnt3a
E
WT (Wnt3a)
Lrp6KO (#1)
Lrp6KO (#2)
Wnt3a
F
WT (Wnt3a)
Lrp5/6dKO (#1)
Lrp5/6dKO (#2)
Wnt3a
G
WT (Wnt3a)
βKO (Wnt3a)
H
0'
20'
28'
71'
125'
I
Stats to WT (Wnt3a)
Wnt bead movement (MSD)
WT (Wnt3a)
WT (iWnt3a)
Lrp5KO (#1)
Lrp5KO (#2)
Lrp6KO (#1)
Lrp6KO (#2)
Lrp5/6dKO (#1)
Lrp5/6dKO (#2)
βKO
+Wnt3a beads
J
Stats to WT (Wnt3a)
Bead retention (% of cells)
Retains
Drops
+Wnt3a beads

Figure 4 - Supplement 1

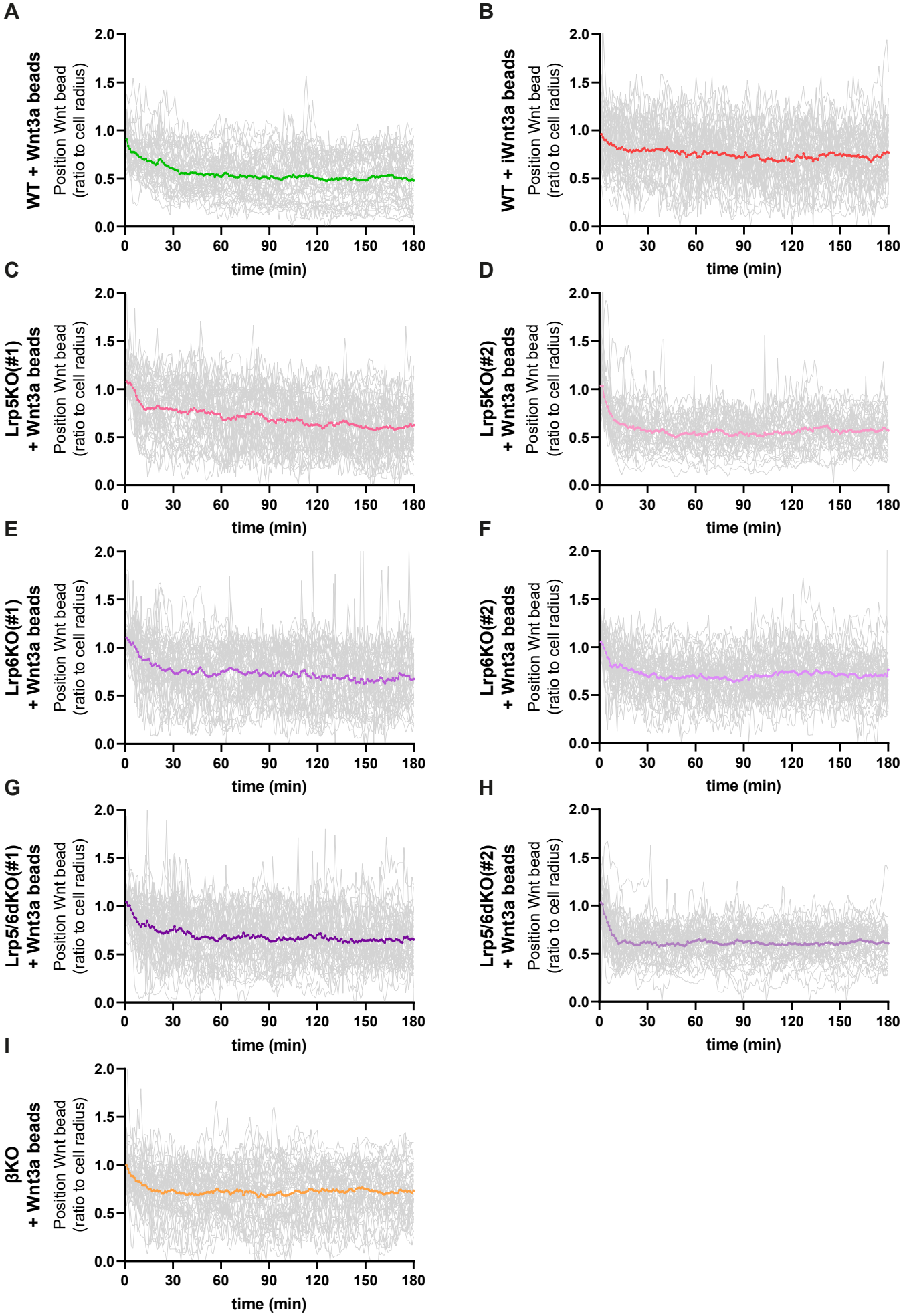

Figure 5

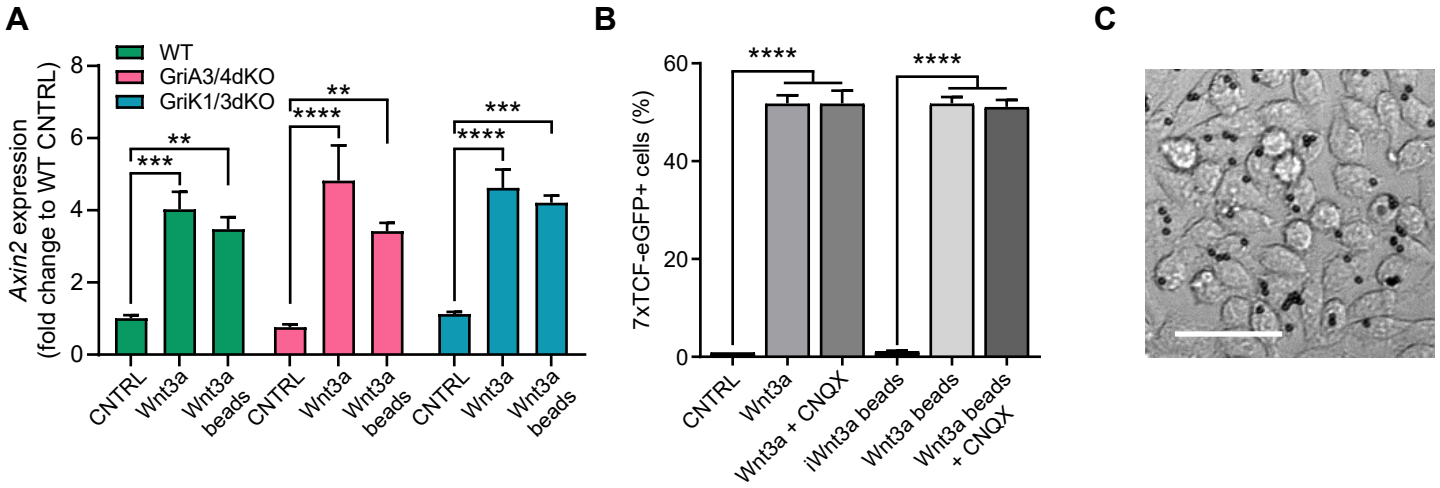
A
WT
GriA3/4dKO
GriK1/3dKO
Axin2 expression
(fold change to WT CNTRL)
0
2
4
6
8
**
***
**
****
***
****
CNTRL
Wnt3a
Wnt3a beads
CNTRL
Wnt3a
Wnt3a beads
CNTRL
Wnt3a
Wnt3a beads
B
7xTCF-eGFP+ cells (%)
0
20
40
60
****
****
CNTRL
Wnt3a
Wnt3a + CNQX
iWnt3a beads
Wnt3a beads
Wnt3a beads + CNQX
C

Figure 5 - Supplement 1

A GriA3/4dKO (#1)

GriA3 (Chromosome X, NC_000086.7) 2bp deletion

```
          GGCGGTCTTCTTTTTAGTCC                CRISPR
5' GCTCCG GGCGGTCTTCTTTTTAGTCC TGG GGCTTTT 3' WT | DNA
5' GCTCCGGGCGGTCTTCTTTTT– –TCCTGGGGCTTTT 3' KO |
```

GriA4 (Chromosome 9, NC_000075.6) 13pb deletion

```
          GGATTTTGGGGACTCGCCAT                CRISPR
5' TTTTCT GGATTTTGGGGACTCGCCAT GGG AGCCTTT 3' WT | DNA
5' TTTTCTGGATTTTGGG–––––––––––––AGCCTTT 3' KO |
```

B GriA3/4dKO (#2)

GriA3 (Chromosome X, NC_000086.7) 2bp deletion

```
          GGCGGTCTTCTTTTTAGTCC                CRISPR
5' GCTCCG GGCGGTCTTCTTTTTAGTCC TGG GGCTTTT 3' WT | DNA
5' GCTCCGGGCGGTCTTCTTTTT– –TCCTGGGGCTTTT 3' KO |
```

GriA4 (Chromosome 9, NC_000075.6) 17pb deletion/ 1bp insertion

```
   GGATTTTGGGGACTCGCCAT                       CRISPR
5' GGATTTTGGGGACTCGCCAT GGG AGCCTTTCCGAG 3' WT |
5' GGATTTTGGGGACTCGC––––––––––––––––G 3' KO | DNA
5' GGATTTTGGGGACTCGC*CATGGGAGCCTTTCCGAG 3' KO |
                    ^
                    C
```

C GriK1/3dKO (#1)

GriK1 (Chromosome 4, NC_000082.6) 107bp deletion

```
          AGACCTCCCCTCAAGTGCTC                CRISPR
5' TTCCTC AGACCTCCCCTCAAGTGCTC AGG ATC 3'     WT | DNA
5' ––––––––––––––––––––––––––AGGATC 3'     KO |
```

GriK3 (Chromosome 16, NC_000070.6) 14bp deletion

```
          CCTCCGGAGTCTGGTTT                   CRISPR
5' GCGGCG CCTCCGGAGTCTGGTTT GGG AATACTG 3'    WT | DNA
5' GCGGCGCCTCCGGAGT––––––––––––––CTG 3'    KO |
```

D GriK1/3dKO (#2)

GriK1 (Chromosome 4, NC_000082.6) 8bp deletion

```
          AGACCTCCCCTCAAGTGCTC                CRISPR
5' TTCCTC AGACCTCCCCTCAAGTGCTC AGG ATC 3'     WT | DNA
5' TTCCTCAGACCTCCCCTCA––––––––GGATC 3'     KO |
```

GriK3 (Chromosome 16, NC_000070.6) 14bp deletion

```
          CCTCCGGAGTCTGGTTT                   CRISPR
5' GCGGCG CCTCCGGAGTCTGGTTT GGG AATACTG 3'    WT | DNA
5' GCGGCGCCTCCGGAGT––––––––––––––CTG 3'    KO |
```

Figure 6

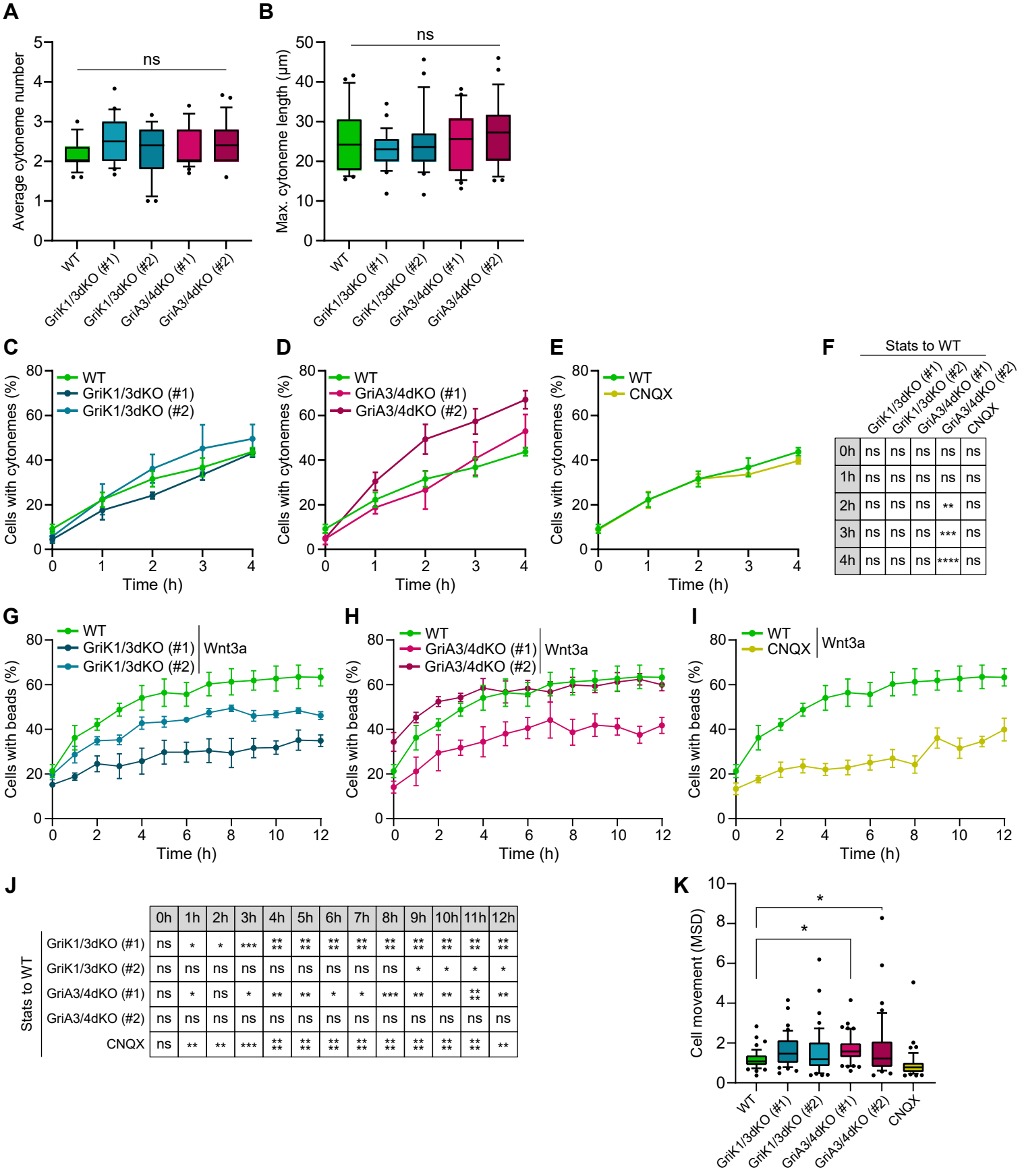

	0h	1h	2h	3h	4h	5h	6h	7h	8h	9h	10h	11h	12h
GriK1/3dKO (#1)	ns	*	*	***	**	**	**	**	**	**	**	**	**
GriK1/3dKO (#2)	ns	ns	ns	ns	ns	ns	ns	ns	ns	*	*	*	*
GriA3/4dKO (#1)	ns	*	ns	*	**	**	*	*	***	**	**	**	**
GriA3/4dKO (#2)	ns	ns	ns	ns	ns	ns	ns	ns	ns	ns	ns	ns	ns
CNQX	ns	**	**	***	**	**	**	**	**	**	**	**	**

Figure 6 - Supplement 1

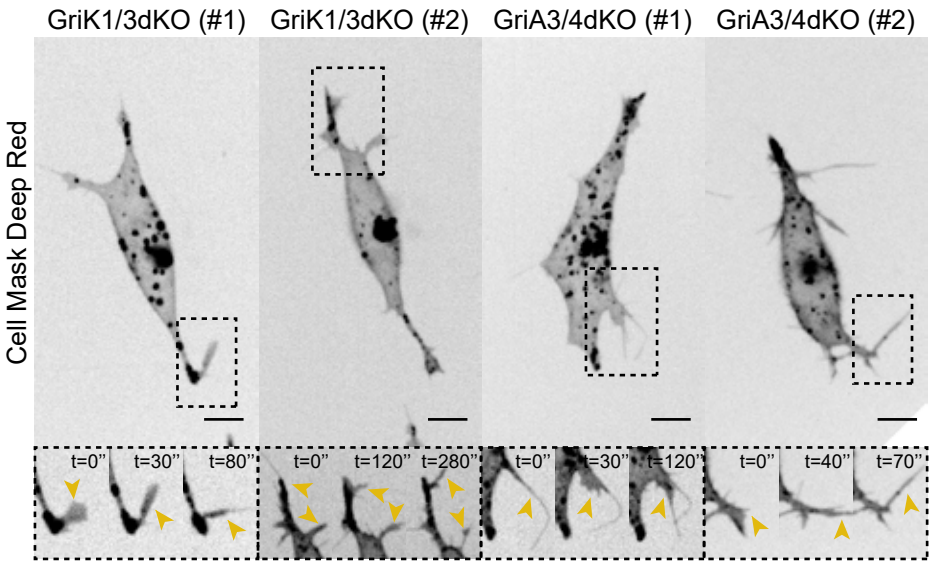

Figure 7

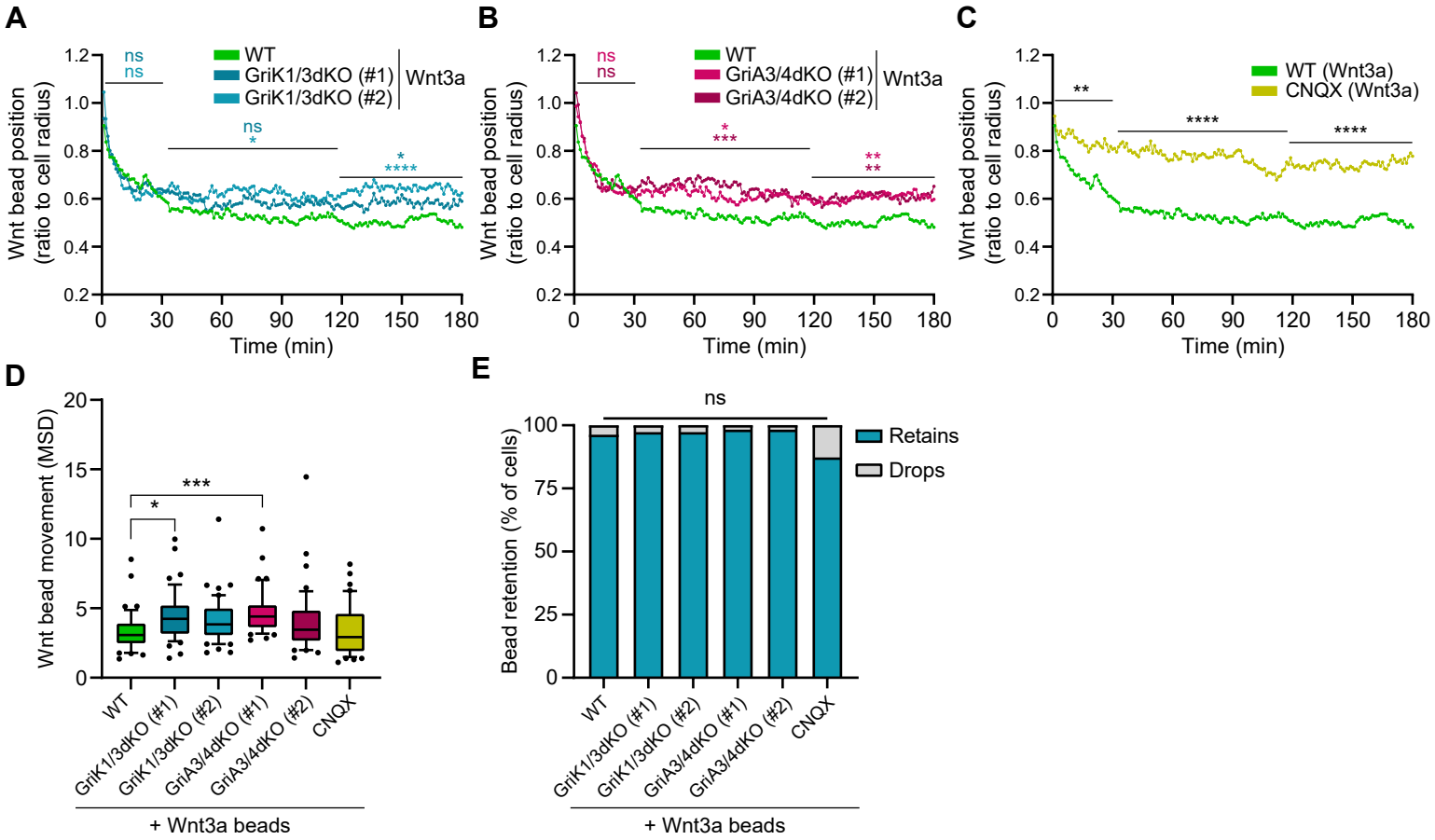
A
Wnt bead position (ratio to cell radius)
Time (min)
WT
GriK1/3dKO (#1)
GriK1/3dKO (#2)
Wnt3a
ns
ns
ns
*
*
****
B
Wnt bead position (ratio to cell radius)
Time (min)
WT
GriA3/4dKO (#1)
GriA3/4dKO (#2)
Wnt3a
ns
ns
*
***
**
**
C
Wnt bead position (ratio to cell radius)
Time (min)
WT (Wnt3a)
CNQX (Wnt3a)
**
****
****
D
Wnt bead movement (MSD)
*
***
WT
GriK1/3dKO (#1)
GriK1/3dKO (#2)
GriA3/4dKO (#1)
GriA3/4dKO (#2)
CNQX
+ Wnt3a beads
E
Bead retention (% of cells)
ns
Retains
Drops
WT
GriK1/3dKO (#1)
GriK1/3dKO (#2)
GriA3/4dKO (#1)
GriA3/4dKO (#2)
CNQX
+ Wnt3a beads

Figure 7 - Supplement 1

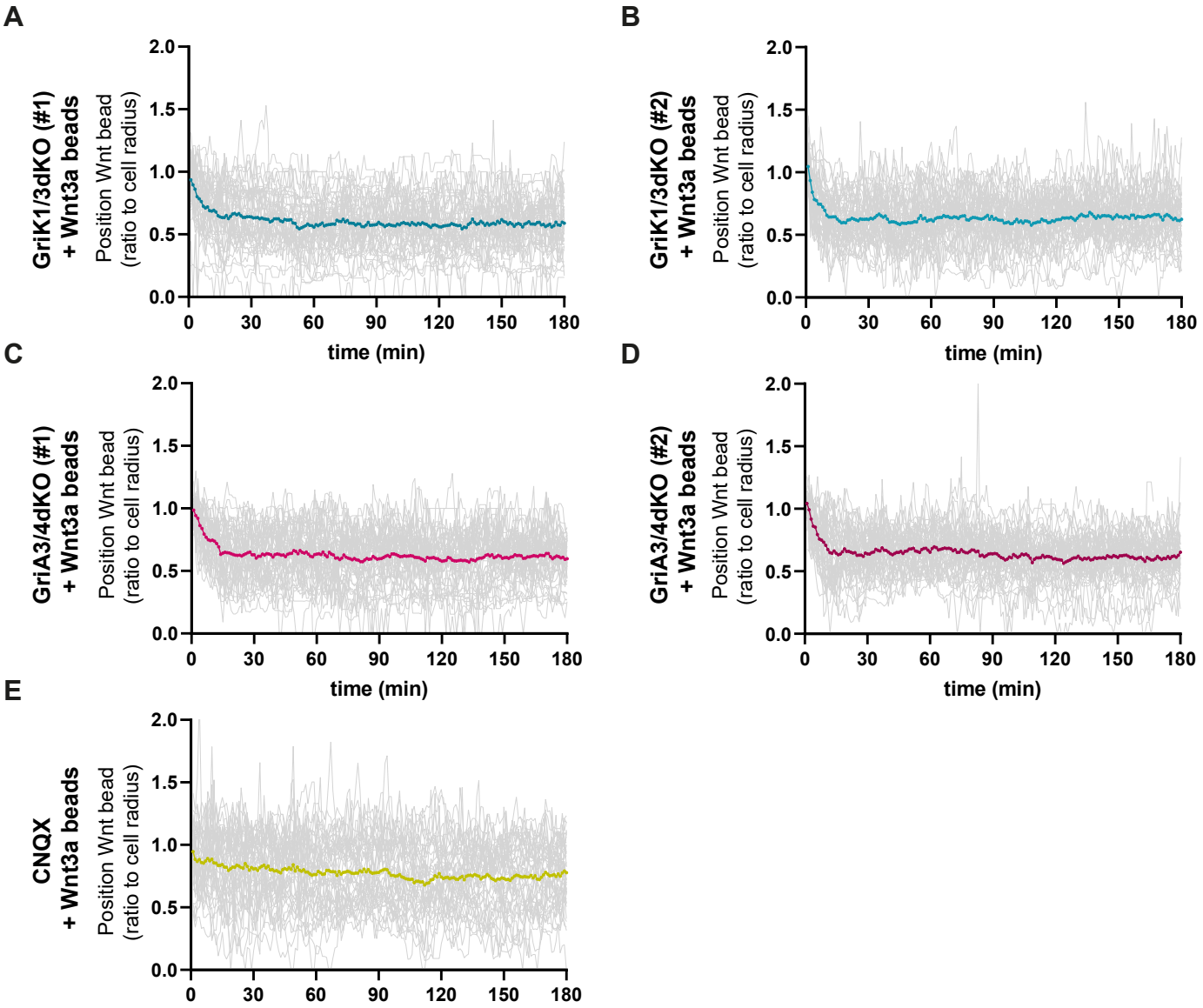

Figure 8

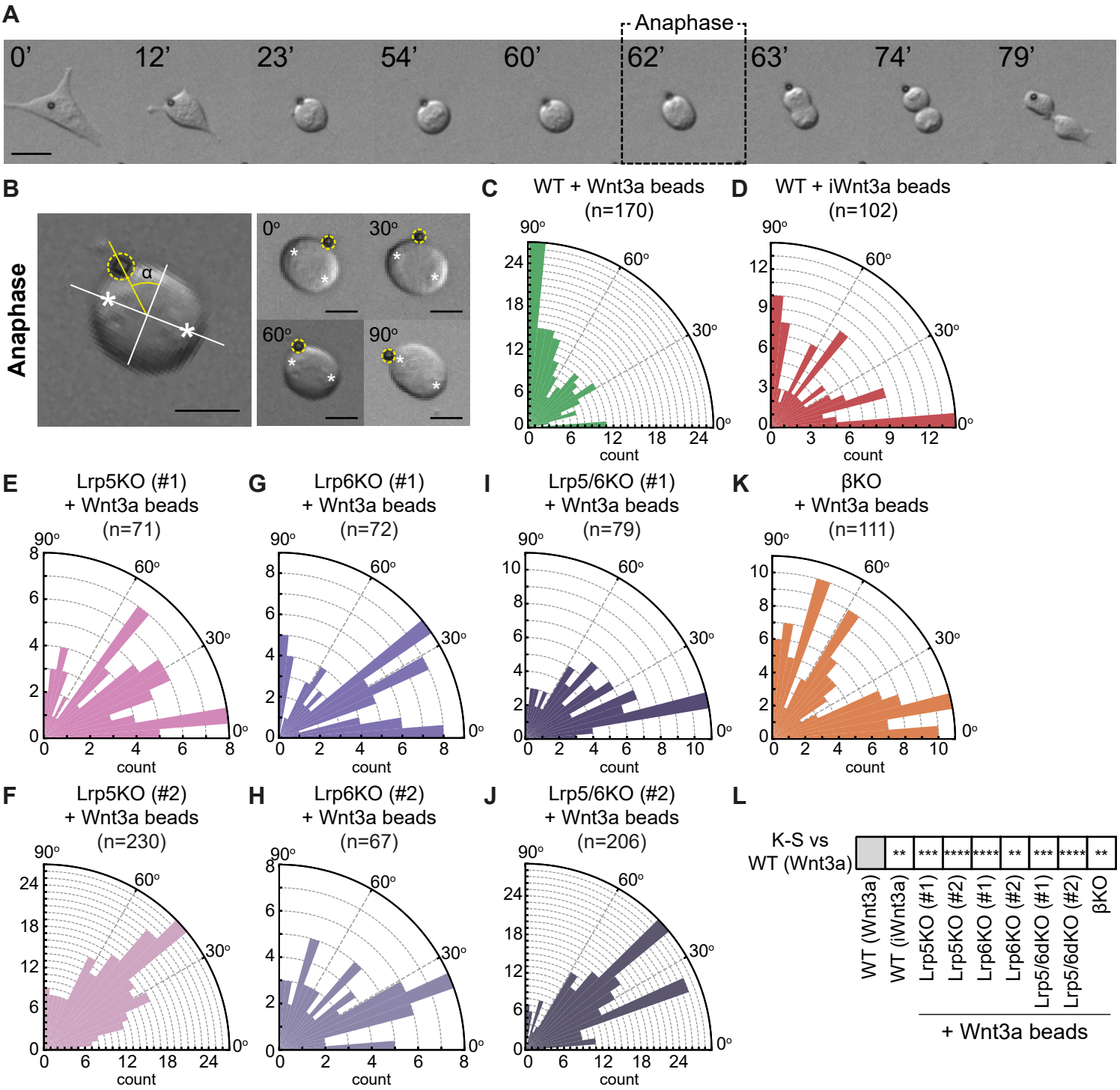
A
Anaphase
0'
12'
23'
54'
60'
62'
63'
74'
79'
B
Anaphase
α
0°
30°
60°
90°
C
WT + Wnt3a beads
(n=170)
D
WT + iWnt3a beads
(n=102)
E
Lrp5KO (#1)
+ Wnt3a beads
(n=71)
G
Lrp6KO (#1)
+ Wnt3a beads
(n=72)
I
Lrp5/6KO (#1)
+ Wnt3a beads
(n=79)
K
βKO
+ Wnt3a beads
(n=111)
F
Lrp5KO (#2)
+ Wnt3a beads
(n=230)
H
Lrp6KO (#2)
+ Wnt3a beads
(n=67)
J
Lrp5/6KO (#2)
+ Wnt3a beads
(n=206)
count
L
K-S vs
WT (Wnt3a)
**
***
****
****
**
***
****
**
WT (Wnt3a)
WT (iWnt3a)
Lrp5KO (#1)
Lrp5KO (#2)
Lrp6KO (#1)
Lrp6KO (#2)
Lrp5/6dKO (#1)
Lrp5/6dKO (#2)
βKO
+ Wnt3a beads

Figure 9

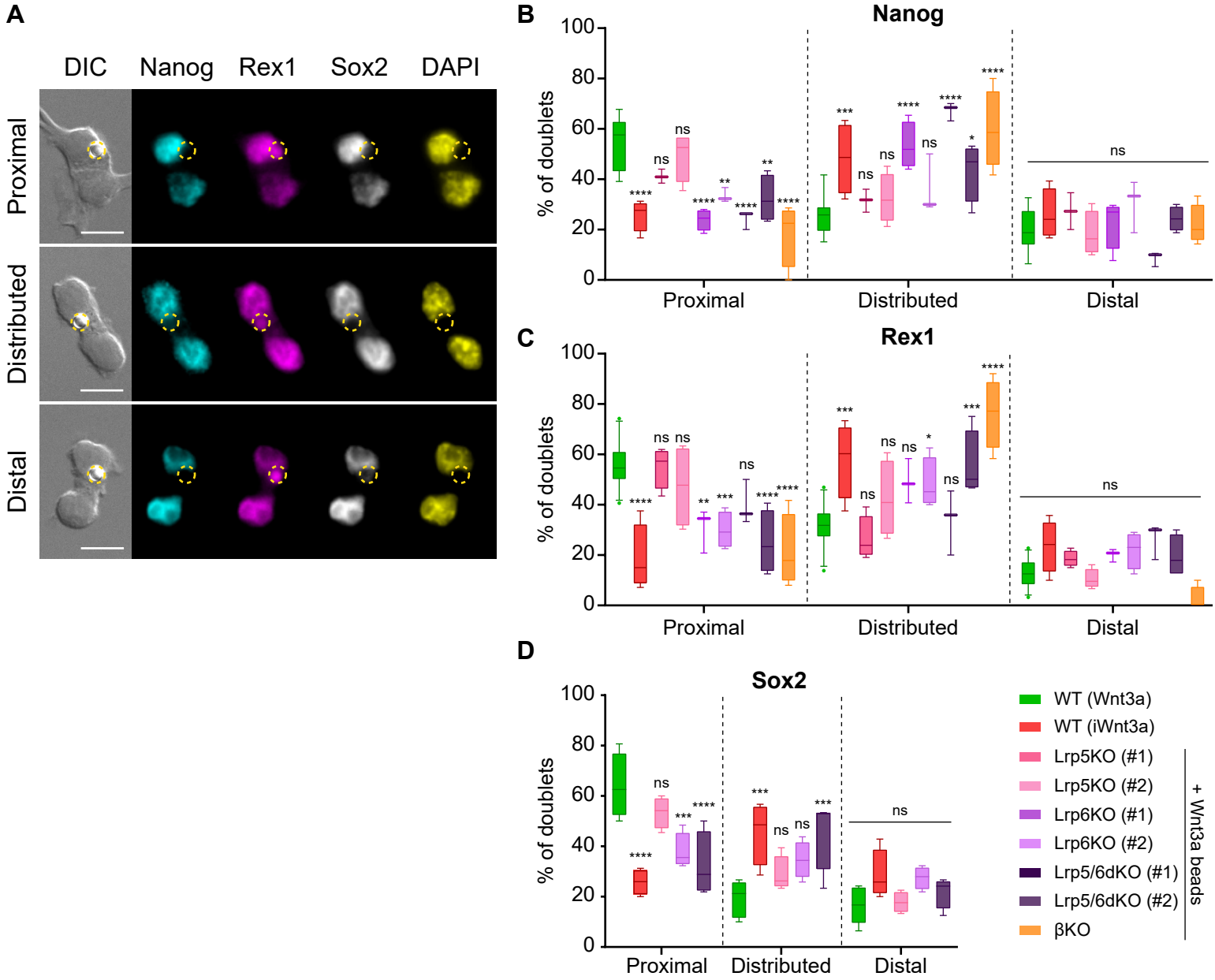
A
DIC
Nanog
Rex1
Sox2
DAPI
Proximal
Distributed
Distal
B
Nanog
% of doublets
Proximal
Distributed
Distal
C
Rex1
D
Sox2
WT (Wnt3a)
WT (iWnt3a)
Lrp5KO (#1)
Lrp5KO (#2)
Lrp6KO (#1)
Lrp6KO (#2)
Lrp5/6dKO (#1)
Lrp5/6dKO (#2)
βKO
+ Wnt3a beads

Figure 10

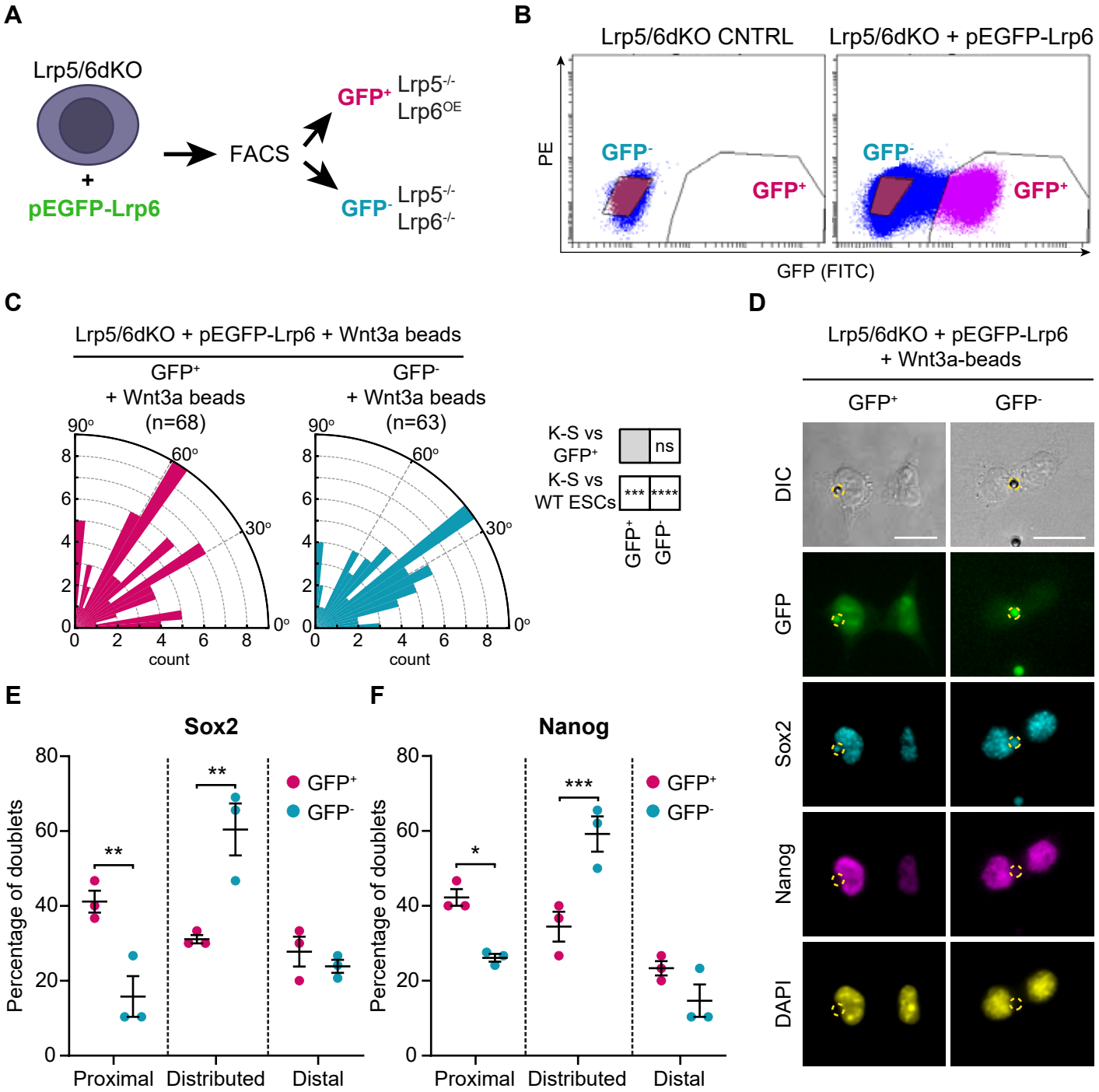
A
Lrp5/6dKO
+
pEGFP-Lrp6
FACS
GFP+ Lrp5-/- Lrp6OE
GFP- Lrp5-/- Lrp6-/-
B
Lrp5/6dKO CNTRL
Lrp5/6dKO + pEGFP-Lrp6
PE
GFP-
GFP+
GFP (FITC)
C
Lrp5/6dKO + pEGFP-Lrp6 + Wnt3a beads
GFP+ + Wnt3a beads (n=68)
GFP- + Wnt3a beads (n=63)
90°
60°
30°
0°
count
K-S vs GFP+
ns
K-S vs WT ESCs
***
****
GFP+
GFP-
D
Lrp5/6dKO + pEGFP-Lrp6 + Wnt3a-beads
GFP+
GFP-
DIC
GFP
Sox2
Nanog
DAPI
E
Sox2
Percentage of doublets
Proximal
Distributed
Distal
F
Nanog

Figure 11

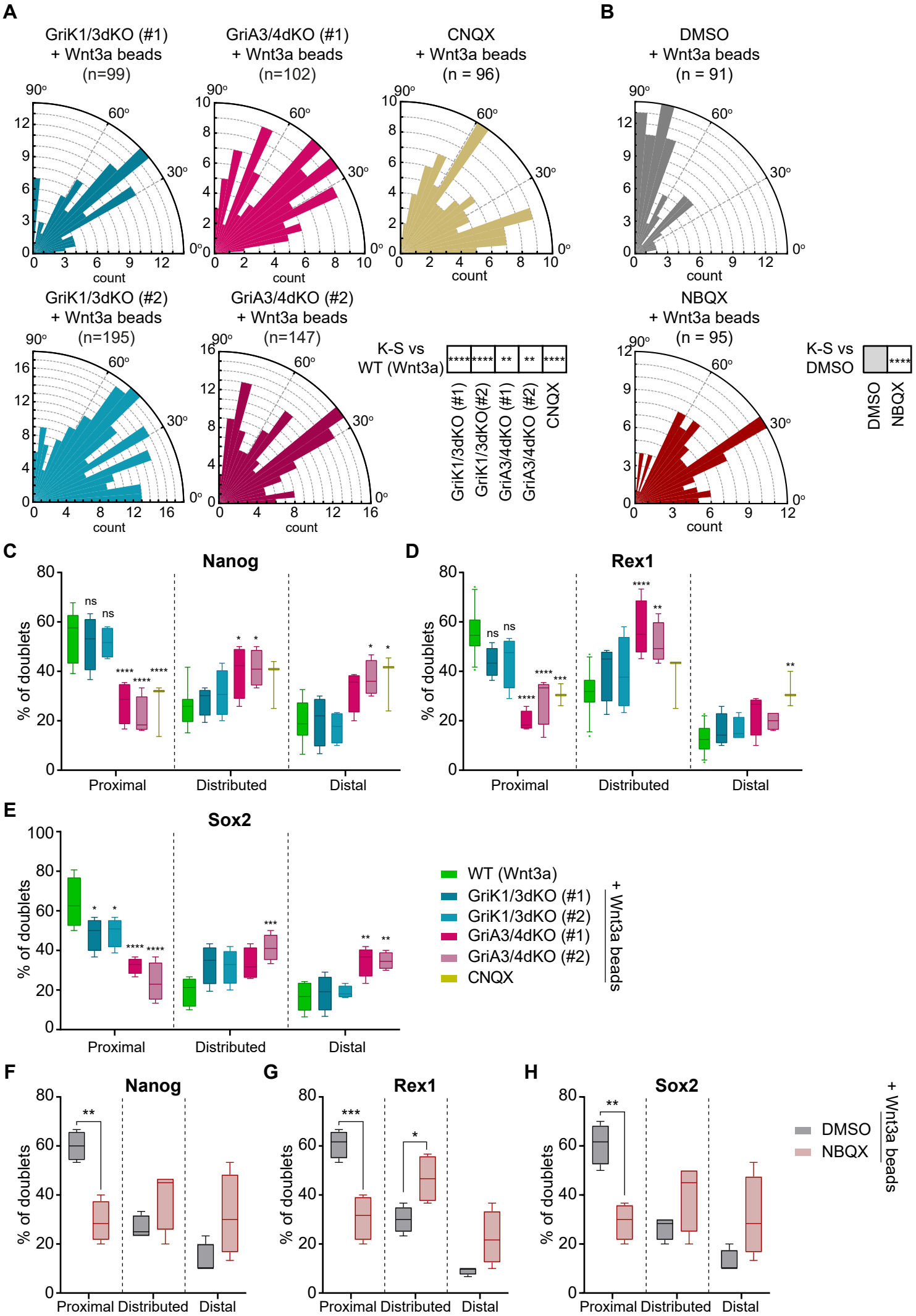
A
GriK1/3dKO (#1)
+ Wnt3a beads
(n=99)
GriA3/4dKO (#1)
+ Wnt3a beads
(n=102)
CNQX
+ Wnt3a beads
(n = 96)
B
DMSO
+ Wnt3a beads
(n = 91)
GriK1/3dKO (#2)
+ Wnt3a beads
(n=195)
GriA3/4dKO (#2)
+ Wnt3a beads
(n=147)
NBQX
+ Wnt3a beads
(n = 95)
90°
60°
30°
0°
count
K-S vs
WT (Wnt3a)
GriK1/3dKO (#1)
GriK1/3dKO(#2)
GriA3/4dKO (#1)
GriA3/4dKO (#2)
CNQX
K-S vs
DMSO
DMSO
NBQX
C
Nanog
D
Rex1
E
Sox2
% of doublets
Proximal
Distributed
Distal
WT (Wnt3a)
GriK1/3dKO (#1)
GriK1/3dKO (#2)
GriA3/4dKO (#1)
GriA3/4dKO (#2)
CNQX
+ Wnt3a beads
F
Nanog
G
Rex1
H
Sox2
DMSO
NBQX
+ Wnt3a beads